Pergamon

Bioorganic & Medicinal Chemistry 8 (2000) 1579–1597

BIOORGANIC & MEDICINAL CHEMISTRY

Conformations in Solution and Bound to Bacterial Ribosomes of Ketolides, HMR 3647 (Telithromycin) and RU 72366: A New Class of Highly Potent Antibacterials

Nathalie Evrard-Todeschi,[a] Josyane Gharbi-Benarous,[a,b] Christine Gaillet,[a] Laurent Verdier,[a] Gildas Bertho,[a] Catherine Lang,[c] Annick Parent[c] and Jean-Pierre Girault[a,*]

[a]*Université René Descartes-Paris V, Laboratoire de Chimie et Biochimie Pharmacologiques et Toxicologiques (UMR 8601 CNRS), 45 rue des Saint-Pères, 75270 Paris Cedex 06, France*

[b]*Université Denis Diderot-Paris VII, UFR Chimie, 2 Place Jussieu, F-75251 Paris Cedex 05, France*

[c]*Hoechst Marion Roussel, 102 route de Noisy, 93235 Romainville Cedex, France*

Received 9 December 1999; accepted 2 March 2000

Abstract—The new class of antibiotics called ketolides is endowed with remarkable antibacterial activity against macrolide-resistant strains. Further modifications of the 3 keto-macrolactone backbone led to 11,12-hydrazonocarbamate ketolides with an imidazolyl–pyridine chain: the file-leader of ketolide class, HMR 3647 (telithromycin), and its *N*-bis-demethyl-derivative, RU 72366. The potency of HMR 3647 is higher than that of RU 72366. Stereospecific ^{1}H and ^{13}C resonance assignments of HMR 3647 and RU 72366 have been determined and have allowed a detailed quantitative conformational analysis of the uncomplexed form of the molecules. The comparative conformation of HMR 3647 in solution and its *N*-bis-demethyl-derivative in D_2O has been carried out using different heteronuclear correlation experiments in conjunction with nuclear Overhauser effect experiments and in particular long-range $^{3}J_{CH}$ coupling constants and using molecular dynamics (MD) methods. The study of ketolide–ribosome interaction has been investigated using two-dimensional transferred nuclear Overhauser effect spectroscopy (TRNOESY). The database of ribosome-bound ketolide structures has been used to compare the structure(s) of ketolide in ribosome–ketolide complexes with the conformational preferences of free ketolides and to highlight the significant differences between HMR 3647 and RU 72366. A comparison of the conformations bound to ribosome was made with those of other previously studied ketolide (RU 004) and macrolides and would explain the remarkable potencies of HMR 3647 in inhibiting protein synthesis.

Introduction

The emergence of bacteria resistant to existing antibacterial agents, including macrolide antibiotics, has accelerated the search for newer and more effective antibacterial agents.[1] The development of the structure–activity relationships is driving the resurgence of interest in macrolides. A series of 3-keto-6-*O*-methyl erythromycin A analogues which lacked the cladinose sugar residue but still maintained potent antibacterial activity[2] against susceptible organisms was developed by Hoechst Marion Roussel.[3–5] In addition this class of macrolides, termed 'ketolides', demonstrated significantly improved activity against MLS (macrolide, lincosamide and streptogramin B) inducibly-resistant organisms.[3,6–8] The C(10)–C(12) position was modified to include cyclic carbamates in the series of 11,12-hydrazonocarbamate ketolides: the previously studied HMR 3004 (RU 004)[9] characterised by a quinoline moiety and the new compounds, HMR 3647[1] and its *N*-bis-demethyl-derivative RU 72366, with an imidazolyl-pyridine chain (Fig. 1). These agents, the ketolides RU 004 and now HMR 3647, have higher in vitro potencies than macrolides and in vivo infection model results with RU 004 (a prototype ketolide) were quite promising.[10] Acid stability experiments of HMR 3647 versus macrolides demonstrate the high stability of ketolides precluding any chemical degradation. HMR 3647 has been shown to be active against a variety of bacteria including macrolide-resistant bacteria and mycobacteria and also to have a good intracellular penetration.[1] All these characteristics of HMR 3647 could result from the

*Corresponding author. Tel.: +33-1-4286-2180; fax: +33-1-4286-8387; e-mail: giraultj@biomedicale.univ-paris5.fr

0968-0896/00/$ - see front matter
PII: S0968-0896(00)00091-2

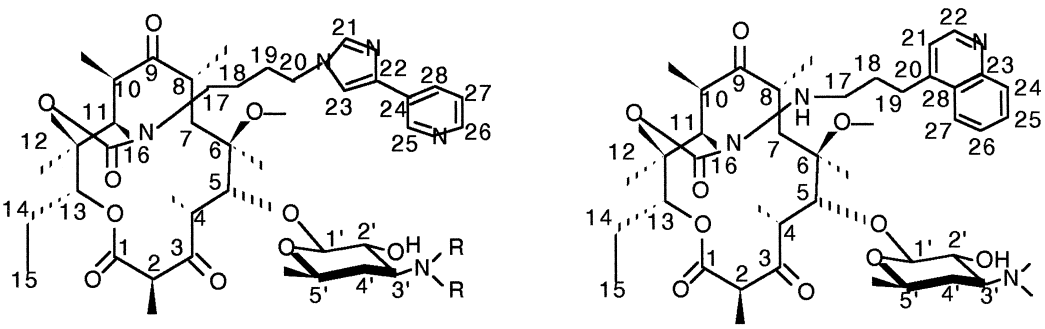

HMR 3647 (1) (R = CH_3)

RU 72366 (2) (R = H)

RU 004 (3)

Figure 1. Structures of three different series of 11,12-hydrazonocarbamate ketolides, a new class of antibiotics: HMR 3647 (**1**), RU 72366 (**2**) and RU 004 (**3**), respectively.

combination of a lipophilic partition coefficient, log $P = 3.3$, and three pK_as herein determined by NMR, that allows HMR 3647 to be more or less protonated depending on the pH of the biological compartment. Some 14-membered ring macrolides cause clinical drug interactions, resulting in altered metabolism of concomitantly administered drugs, via formation of an inactive and stable cytochrome P-450 complex.[11] Unlike macrolides, HMR 3647 does not form any detectable metabolic intermediate complex (nitroso-complexes were detected neither in vitro nor in vivo). Thus, little or no drug–drug interaction is expected with ketolides.[3] HMR 3647 was selected to be the ketolide candidate with low toxicity and a favourable pharmacodynamic profile for the clinical trials, to be put on the market as telithromycin.

In this article, we will try to shed light on the conformation of HMR 3647 free in solution and bound to bacterial ribosomes. The mechanism of action of ketolides has been observed to be similar to that of the macrolides, i.e., by means of binding to the 50S ribosomal subunit[12–14] and subsequent inhibition of bacterial protein synthesis.[4,15] Macrolides, ketolides and lincosamides exert their antibacterial action by binding to bacterial ribosomes, specifically to the 50S subunit. Two different types of antibiotic–ribosome specific interactions exist with the 50S ribosomal subunit: (i) strong interaction ($K_d = 10^{-7}$–10^{-9} M)[17–19] only measured by equilibrium dialysis and related methods, and (ii) weak interaction ($K_d = 10^{-3}$–10^{-5} M) characteristic of a biological activity which can be detected by NMR spectroscopy and studied by transferred nuclear Overhauser effect measurements (TRNOE).[16,17] The weakly bound state of the ketolide studied here represents a first stage in an allosteric two-stage binding process.[9] The weak interaction observed by NMR TRNOE experiments could be involved in the first step of recognition and selection of antibiotics by the ribosomal machinery, the second step being the strong interaction responsible for the protein biosynthesis inhibition.[18]

If binding is sufficiently weak to allow exchange (fast on the time scale of spin-lattice relaxation rate), TRNOE NMR experiments[19–24] are well adapted to study the bound conformation in a ligand–receptor complex transferred to the free molecule via chemical exchange. Thus the tight binding of antibiotics to ribosomes cannot be characterized by NMR spectroscopy unlike the weak interaction which is a fast exchange process on the NMR.

The weak interaction was only observed with macrolide antibiotics which have shown good activity. Compounds which are not able to take part in a weak binding interaction with bacterial ribosomes do not exert antibiotic activity,[25] which was also observed by Barber et al.[18,26] Thus, the weak binding site seems to be a necessary step for the strong interaction. Unlike their parent compounds in vivo, roxithromycin and erythromycin A metabolites do not retain antimicrobial activity. Consequently, they are not able to take part in a binding interaction with bacterial ribosomes. These inactive metabolites showed very little line broadening and at the same time gave essentially blank TRNOESY spectra.[25]

To distinguish between the specific effects of binding drugs to their targets and non-specific interactions, ribosomal 'core' particles were prepared by incubating 50S subunits with 1.3 M LiCl solution to remove outer proteins,[27] then cores were used in place of whole ribosomes with antibiotics in control experiments. The addition of ribosomal cores results in only a slight broadening of all the lines in the control spectrum, which was characteristic of only non-specific interactions between antibiotics and ribosomal core particles.

Several antibiotics including 14-membered macrolides like erythromycin and roxithromycin, 16-membered macrolides like spiramycin and josamycin, ketolides like RU004,[9] and lincosamides like lincomycin and clindamycin[28] inhibit protein synthesis by interfering with

the peptidyl-transferase function of the 50S ribosomal subunit.[29–31] Earlier work[32,33] on the strong interactions of lincomycin has given rise to the conclusion that lincomycin and streptogramin A only interact with free ribosomes and 50S subunits and block the early rounds of peptide bond formation prior to polysome formation, while erythromycin and streptogramin B prebind to the ribosome and block peptide elongation. The lincosamide conformations when weakly bound to bacterial ribosomes were determined from the TRNOE experiments.[28] Superimposition of lincosamide and macrolide bound structures exhibited conformational similarities in a particular fragment, which is in agreement with a hypothesis of partial overlapping lincosamide and macrolide binding sites.[28] In the ribosome complex, from the constraints of the different TRNOEs observed in D_2O, the lincosamide and macrolide families present a shared bound region when weakly bound to bacterial ribosomes. In the present study, we have taken advantage of transferred nuclear Overhauser effects to gain information about the conformation of HMR 3647 and RU 72366 in the bound state and to compare their weak interaction responses.

It was noticed that ketolide RU 004 showed a higher affinity for the 70S ribosome target than did macrolides[9] and displayed a significantly better overall antibiotic activity. Thus, in the ribosome complex, from the constraints of the different TRNOEs observed in D_2O solvent, we propose to analyse whether the active molecules belonging to ketolide and macrolide class present a shared bound region or if the conformations weakly bound to bacterial ribosomes may be varying.

Results and Discussion

Structural characteristics of the free ligands

HMR 3647's physicochemical properties remain to be fully characterised and we herein report on the structural characteristics with respect to their biological properties. In order to compare the behaviour of HMR 3647 and its *N*-bis-demethyl-derivative, the primary goal of this work was to determine the overall solution conformation of the free drugs.

NMR spectroscopy. A combination of NMR studies and molecular modelling has been used to predict the major conformations of HMR 3647 and RU 72366 in solution and their similarity to the conformations of the crystalline structure (Figs 2 and 3), the ketolide RU 004 and the 14-membered-ring macrolides. The identities and proportions of the different isomers in aqueous solution were of special interest. This was accomplished by obtaining information about dihedral angles from the vicinal coupling constant data, by acquiring the spatial proximity information from nuclear Overhauser effect data and through the use of molecular modelling by dynamics calculations. It is first necessary to assign the ^1H and ^{13}C NMR spectra of the drug.

Assignment of the ^1H and ^{13}C NMR spectra. HMR 3647 was much more soluble in D_2O solution than RU 004, the previously studied ketolide and than RU 72366. Since it was not possible to obtain useful ^{13}C spectra of RU 72366 in D_2O solution, D_2O buffer:DMSO-d_6 (97:3) solutions were used. The ^1H and ^{13}C NMR chemical shifts in D_2O solution at apparent physiological pH 7.6 for **1** and **2** are listed in Table 1.

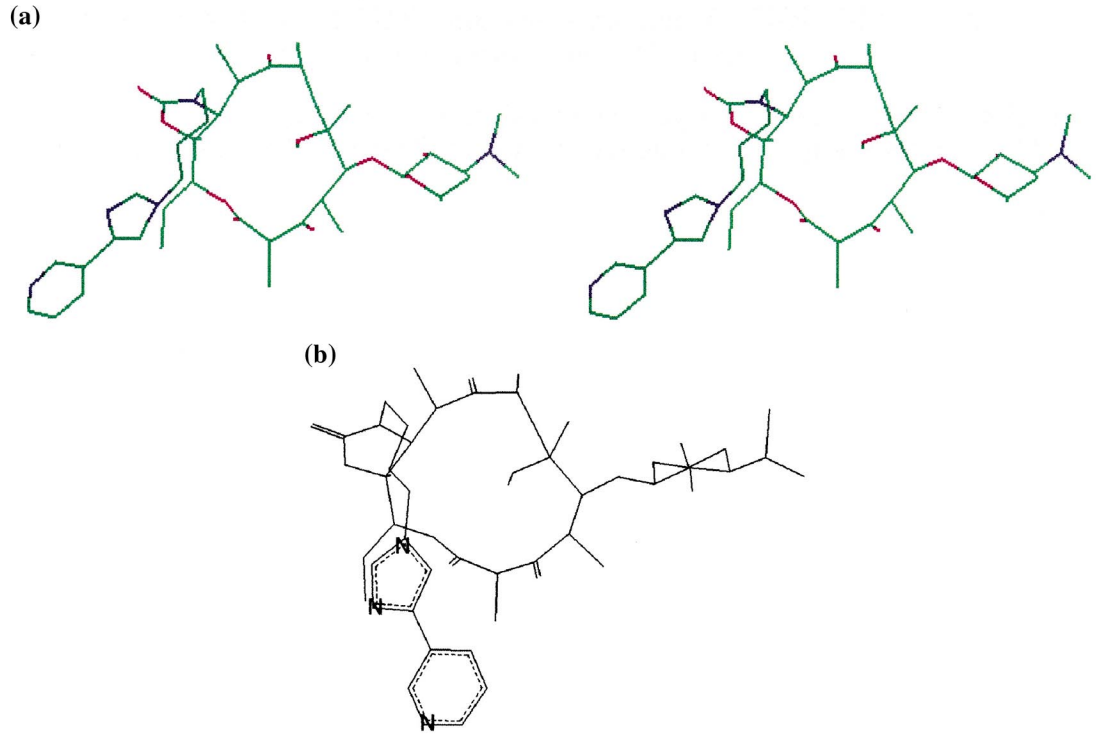

Figure 2. (a) Stereoviews of X-ray structure from crystal data of HMR 3647 (**1**). (b) The minimised X-ray structure $S1^{-}$–Z (176.6 kcal mol^{-1}) from crystal data of HMR 3647 (**1**) is characterised by a **C1** position of the aromatic imidazolyl–pyridine chain in the S^{-}–Z structure. The **C1** chain seems to be pushed back towards the left part of the macrocycle, in the C(11)–C(13) region.

Table 1. ^{1}H and ^{13}C NMR spectra of HMR 3647 (**1**) and RU 72366 (**2**) in D_2O buffered solutions

	HMR 3647		RU 72366	
Site	δ_H[a]	δ_C[a]	δ_H[a]	δ_C[a]
1		173.9		173.0
2	4.19	51.8	[b]	52.6
2-Me	1.22	17.5	1.23	16.6
3		210.9		209.7
4	3.20	47.7	3.20	48.7
4-Me	1.19	19.9	1.18	15.3
5	4.02	81.6	4.02	80.9
6		80.5		79.5
6-Me	1.07	21.9	1.07	21.0
6-OMe	2.11	51.8	2.13	50.8
7a (*proR*)	1.75	41.5	1.74	40.6
7b (*proS*)	1.66		1.66	
8	2.52	46.0	2.52	48.7
8-Me	1.18	15.9	1.18	18.9
9		224.4		223.2
10	3.29	41.7	3.28	41.0
10-Me	0.98	16.3	0.98	14.9
11	3.47	64.1	3.46	63.1
12		86.9		85.9
12-Me	1.57	16.5	1.57	15.5
13	4.76	80.6	4.75	79.6
14a	1.64	24.9	1.63	23.8
14b	1.79		1.80	
15-Me	0.79	12.6	0.79	11.7
16		162.0		160.5
17a	3.60	45.9	3.59	45.0
17b	3.60		3.55	
18a	1.46	26.6	1.45	25.6
18b	1.46		1.45	
19a	1.89	30.3	1.89	29.3
19b	1.82		1.75	
20a	4.20	49.6	4.20	48.7
20b	4.09		4.08	
21	7.77	141.8	7.77	140.7
22		140.2		139.1
23	7.68	119.9	7.69	118.9
24		132.7		132.0
25	8.85	147.6	8.85	146.6
26	8.43	149.6	8.43	148.6
27	7.53	127.2	7.53	126.3
28	8.15	135.8	8.15	134.8
1′	4.38	105.1	4.36	104.2
2′	3.48	71.6	3.29	73.8
3′	3.43	67.8	3.29	53.6
3′-N(Me)$_2$	2.82	42.0	—	—
4′-ax	1.55	32.3	1.46	38.0
4′-eq	2.14		2.15	
5′	3.78	71.6	3.77	70.9
5′-Me	1.32	22.6	1.28	21.5

[a]Solutions in buffered D_2O at pH 7.6: 4 mM of HMR 3647 and 2 mM of RU 72366.
[b]Protons are exchanged with solution (probably by tautomerism).

The TOCSY[34] and the COSY spectra were used to distinguish the spin groups and to confirm the assignments of the hydrogen resonances within each spin group. The chemical shifts of the *N*,*N*-dimethyl protons will depend on the state of ionisation of that group and varying the pH allows us to determine by NMR the pK_a value of the amino function, pK_a = 8.7 for **1** and 8.1 for **2** (dimethylamine). In D_2O solution at pH 7.6, the amino group signal of HMR 3647 at 2.82 ppm is similar to the resonance of the methyl in the protonated form.

The assignments were obtained using 1D ^{1}H and ^{13}C (^{1}H decoupled and DEPT-135)[35] spectra, 2D homonuclear double quantum (COSY) spectra, heteronuclear multiple bond correlation (HMBC) spectra[36] and heteronuclear multiple quantum bond correlation (HMQC) spectra.[37]

A number of signals could be readily assigned. The high frequency signals were assigned, respectively, to the imidazol and pyridine protons. Following their chemical shifts when varying the pH, the two imidazol and pyridine pK_as were determined, pK_a = 4.8 (imidazol) and pK_a = 2.1 (pyridine), for **1** and **2**. The strong NOE [CH_2-17]10-Me is the only possibility to link the macrocycle to the imidazolyl-pyridine chain for a completely unambiguous assignment. It remained to assign the quaternary carbon of the imidazolyl-pyridine side chain C(22), C(24) thanks to HMBC experiments.

The methyl group CH_3(2) appears as a singlet because the H(2) was exchanged in D_2O, presumably in the tautomeric equilibrium of the β-keto-ester enolate form. In the HMBC spectrum C(2) was assigned from CH_3(2). The CH_3(6) and OCH_3(6) methyl group remained to be assigned. The HMBC spectrum showed cross peaks from C(6) to the methyl groups surprisingly at δ_H 1.07 and 2.11 for HMR 3647 and δ_H 1.07 and 2.13 for RU 72366 in D_2O. These signals were assigned to CH_3(6) and OCH_3(6), respectively. The upfield shifts seen for CH_3(6) and OCH_3(6) (^{1}H spectrum) resonances are caused by the shielding effect of the stacking interactions with the two imidazol and pyridine aromatic nucleus. Indeed, working at constant temperature and varying the pH, the CH_3(6) and OCH_3(6) chemical shifts are observed to depend on the state of ionisation of these units.

Concerning RU 72366, the ^{1}H chemical shifts do not differ significantly from HMR 3647, except for an increase for protons of the chain, H(17) and H(19), which could be related to a different position of the imidazolyl-pyridine moiety. In the same way, an important effect (+0.08–0.18 ppm) is naturally appearing for the desosamine sugar signals due essentially to the *N*-bis-demethylation of the amino group at C(3′). The variations of ^{13}C chemical shifts are observed around the C(4) region for C(4) and C-Me(4) (−1 and +5 ppm, respectively) but also at the regions around C(8), −2 and −3 ppm, respectively, for C(8) and C-Me(8) due perhaps to some slight fluctuation of the two carbonyl groups (3-CO and 9-CO) with respect to the macrocycle. For RU 72366, the shifts in ^{13}C assignments with the largest amplitude were caused by the perturbation around the C(3′) region. The shifts are quite consistent with the different pK_a value in D_2O solution of the 3′-amino groups but also with hydrogen bonding (or not), so that the high field shift of C(3′) (−14 ppm) in RU 72366 relative to HMR 3647 is most probably due to intramolecular hydrogen bonding involving the amino group at C(3′) to the hydroxyl at C(2′), NH_3^+(3′)///OH(2′), as observed in RU 72366 by molecular modelling calculations.

Homonuclear $^3J_{^1H-^1H}$ and heteronuclear $^3J_{^{13}C-^1H}$ coupling constants. The determination of $^3J_{HH}$ and long-range $^3J_{^{13}C-^1H}$ coupling constants[38] shown in Table 2 was used to predict the conformational analysis of the flexible units (macrocycle, imidazolyl-pyridine chain and particularly desosamine sugar). This is especially important for the torsion angles of the glycosidic bonds Ψ_1 = H(5)–C(5)–O(5)–C(1′) and Ψ_2 = H(1′)–C(1′)–O(5)–C(5) studied by selective excitation of the protons H(5) and H(1′), respectively. Our observed values were compared to those calculated by using Karplus-type equations[39,40] from minimised structures, generated by MD study (Table 2).

An analysis of the $^3J_{H,H}$ values was also used to compare the major solution state conformation of HMR 3647 with that in the crystalline state. The observed vicinal coupling constants confirm that HMR 3647 exists in solution as a major conformation which is very similar to the solid state conformation (Table 2).

Concerning the values of homonuclear ^3J coupling constants, one can see that the lactone ring conformation is not significantly perturbed except for slight deviations relative to the $^3J_{4,5}$ values for ketolide compounds, RU 004, HMR 3647 and RU 72366 (8.2, 7.9 and 7.7 Hz, respectively). Two types of conformations have to be considered: (i) type '**M2**' with a transoidal angle in an eclipsed Newman projection (ca. 120°), (H(4)–C(4)–C(5)–H(5), *eclipsed*), 3-CO 'exo' with H(4) 'folded in' and Me(4) 'down' and (ii) type '**M1**' with a trans-pseudo-axial angle (ca. 170°), (H(4)–C(4)–C(5)–H(5), *trans*), 3-CO 'up' with H(4) 'down' and Me(4) 'folded out', respectively (Fig. 4a). The coupling constants found (Table 2) for H(4)–C(4)–C(5)–H(5) are consistent with the predominant **M1** conformation and a slight participation of the **M2** one. The observed $^3J_{13,14}$ (≈10 Hz) coupling constants relative to C(13)–C(14) reveals that the ethyl group is in a major *trans* **T1** form with a participation of the minor (g^-) **T2** and (g^+) **T3** ones (Fig. 4b).

The measurement of heteronuclear long-range $^3J_{^{13}C-^1H}$ coupling constants (Table 2) by selective 2D INEPT[38] combined with studies by MD was useful to identify the positions and mobility of the sugar moiety with respect to the erythronolide (Fig. 4c). Experimental values ($J_{\Psi1}$ = 3.9 and 4.4 Hz and $J_{\Psi2}$ = 1.0 and 2.0 Hz) are discussed with regard to the calculated values in the different '**D1**–**D4**' conformers from lowest energy structures (Table 2). The desosamine sugar can adopt either conformations '**D1**' or '**D2**' ($J_{\Psi2}$≈2.0 Hz) with an orientation perpendicular to the macrocyclic lactone ring or conformations '**D3**' ($J_{\Psi2}$≈5.2 Hz) and '**D4**' ($J_{\Psi2}$≈3.8 Hz) with the two units in the same plane (Fig. 4c). The observed values for $J_{\Psi1}$ (3.9, 4.4) and $J_{\Psi2}$ (1.0, 2.0) in

Table 2. Vicinal coupling constants (^3J Hz) for HMR 3647 (**1**) and RU 72366 (**2**) in D_2O buffered solution and calculated coupling constants obtained from the different conformations generated by MD according to the notation for macrocycle **M**, desosamine **D** and ethyl **T**

	J_{exp}		J_{calc}				J_{calc}
Vicinal pair	**1**	**2**	**M1**	**M2**			**S** X-ray
J (macrocycle)							
H4–H5	7.9	7.7	12.3	3.3			12.3
H5–C3	≤2.0		2.5	4.9			3.5
H5–Me6	≈1.0		1.5	1.5			2.3
H8–H7a (7*pS*)	12.1	11.8	12.4	12.4			12.4
H8–H7b (7*pR*)	2.2	2.3	2.4	2.3			2.3
H10–H11	1.5	≤1.0	1.7	2.2			1.5
J (desosamine)			**D1**	**D2**	**D3**	**D4**	
H5–C1′	3.9	4.4	5.4	4.6	4.9	5.2	5.0
C5–H1′	≈1.0	≤2.0	2.2	2.5	5.2	3.8	1.1
H1′-H2′	6.9	7.0	9.9	9.9	9.9	9.9	9.9
H2′–H3′	10.6		10.0	10.0	10.0	10.0	10.0
H3′–H4′eq	4.0	4.6	3.5	3.5	3.6	3.5	3.5
H3′–H4′ax	11.7		11.4	11.4	11.4	11.4	11.4
H4′eq-H5′		1.8	3.8	3.8	3.8	3.8	3.8
H4′ax-H5′	10.3		11.1	11.1	11.1	11.1	11.1
J (ethyl group)			**T1**	**T2**	**T3**		
H13–H14a (14*pS*)	10.0	9.9	12.3	2.0	1.9		12.3
H13–H14b (14*pR*)	2.7	3.0	2.4	12.3	6.6		3.2

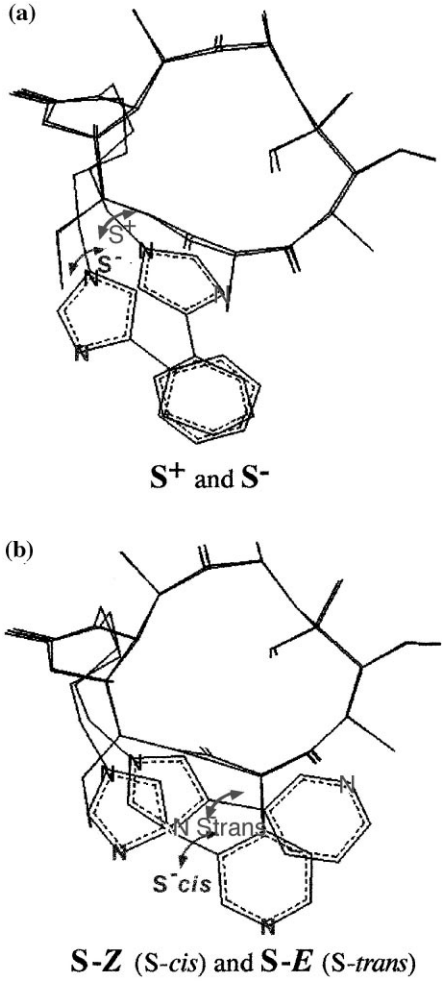

Figure 3. (a) The structures are referred to S^+ or S^- because the last rotor corresponding to the alkyl part of the chain, the C(18)–C(21) torsion angle, is either g^- (S^-) or g^+ (S^+). (b) The structures are referred to *S–Z* or *S–E* because the two nitrogen atoms corresponding to the imidazolyl-pyridine part of the chain, the C(23)–C(28) torsion angle, is either *eclipsed* (*S–Z*) or *anti* (*S–E*).

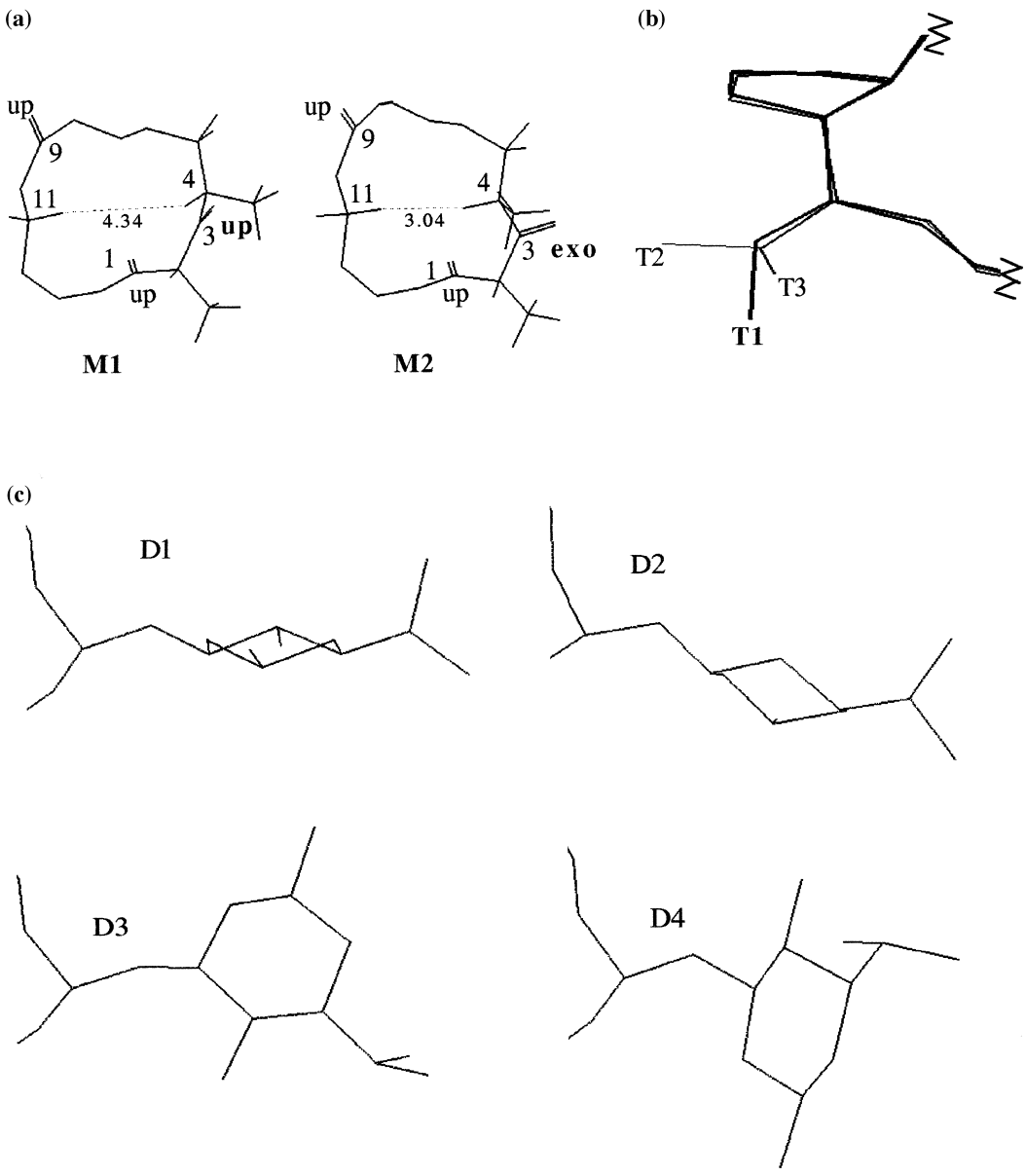

Figure 4. (a) The conformer **M1** was characterized by the 'up' position of the three carbonyl groups (1-CO, 3-CO and 9-CO). An 'exo' orientation of the 3-CO groups leads to **M2,** with a 'down' orientation of the 4-Me. (b) The ethyl group leads to three **T1**–**T3** positions: parallel (*t*) **T1** and perpendicular (g^-) **T2** and (g^+) **T3** to the macrocycle. (c) Conformations of the desosamine sugar ring following its orientation with respect to the lactone ring and the glycosidic dihedral angles, ψ_1, H(5)–C(5)–O(5)–C(1′), ψ_2, C(5)–O(5)–C(1′)–H(1′): two orientations are perpendicular to the macrocycle: **D1** (ψ_1, 10°, ψ_2, 55°) and **D2** (induced by the **M2** conformer) (ψ_1, 25°, ψ_2, 50°); in the **D4** (ψ_1, 15°, ψ_2, 140°) position, the desosamine sugar is coplanar to the macrocycle with a 'turn back' of 180° relative to the orientation **D3** (ψ_1, −20°, ψ_2, −10°).

Table 2 should include a large participation of conformer perpendicular '**D1**' or '**D2**'.

All these conclusions will be further tested using MD experiments.

Nuclear Overhauser enhancement (NOE). Typical contacts through space are reported in Table 3 for the two compounds. The 2D ^{1}H NOESY map in D_2O buffered solution (≈ 2 mM) at pH 7.6, with a mixing time, $\tau_m = 150$ ms, is empty. In the NOESY spectrum with $\tau_m = 800$ ms, only few and weak positive NOEs were identified. They indicate that the macrocycle lactone ring will better correspond to the major '**M1**' conformation since some NOEs expected for models '**M2**' are missing in the HMR 3647 and RU 72366 solution, particularly the large NOEs [6-OMe]4, [6-OMe]8, [6-OMe]13, [12-Me]4 and especially [11]4. The [15-Me]2-Me NOE corresponds to a parallel orientation **T1** of the ethyl unit in HMR 3647. Analysis of NOEs for HMR 3647 and RU 72366 does not show interesting macrocycle/imidazolyl-pyridine chain inter-unit contacts. There is not any contact between the chain and the erythronolide in HMR 3647 indicating probably a total release of the chain. Whereas, for RU 72366 molecule, connectivities from the beginning of the chain, [18]6-OMe and [20]2-Me, are observed, suggesting that the chain is pushed back toward the right part of the macrocycle in the C(2)–C(6) region (Fig. 5). At the same time, for RU 72366 no contact exists between

Table 3. Observed NOEs and TRNOEs for HMR 3647 (**1**) and RU 72366 (**2**) in D_2O solution. Inter-proton distances from minimized structures derived from MD

Connectivities[a]	NOEs[b]		TRNOEs[c]		Inter-proton distances[d]					
Intra-macrocycle	(**1**)	(**2**)	(**1**)	(**2**)	**M1**	**M2**				
5–4Me			s	m	s	m				
6Me–4			w		w	w				
6OMe–4			w		w	m				
6OMe–4Me			m	m	w					
7–5			m		m	m				
7–6OMe			s	w	w	w				
8–6OMe			w		w	m				
8Me–6Me				s	w	w				
10–6Me				w	w					
11–4			m	w	w	m				
11–6OMe		w	s	m	s	s				
11–7	w		m		m	m				
11–8Me			s	w	w	w				
11–10Me			m	w	m	m				
12Me–4			w	w	w	m				
12Me–8Me			s	s	m	w				
13–6OMe			w		w	m				
	(**1**)	(**2**)	(**1**)	(**2**)	**T1**	**T2**	**T3**			
15Me–2Me	m		m	m	s		w			
15Me–11			w		w					
15Me–12Me			m	m	w	m	m			
15Me–13			s	m	s					
Chain-macrocycle	(**1**)	(**2**)	(**1**)	(**2**)	**C1**$^+$–*Z*	**C2**$^+$–*Z*	**C2**$^+$–*E*	**C3**$^-$–*Z*	**C3**$^-$–*E*	**C4**$^-$–*Z*
17–6OMe			m	w	w	m	w	s	m	w
17–13			m			m	w	m	w	w
18–6OMe		w	s	s		s	m	m	m	s
18–10Me		w	w		w	w	w			w
18–10				m		w	w		m	w
18–11			s	m	m	s	m	s	w	s
18–13			m		w	s	m	s	s	m
19–6OMe			m	m	s	s	w	m	w	w
20–6OMe		w	w		s	w	w	w	w	m
21–6Me			w							w
21–6OMe			w	w	s	m	m	m		m
21–15Me			w		w			m	s	
23–6Me			w					w		m
23–6OMe			w	w		m	w	m	m	m
23–15Me			w	w		s	s			
23–17			w	w	w			w	w	m
23–18			m	w	s	s	m	w	m	m
25–2Me			w	w		m	m	m		
25–6OMe			w	w		w		w	s	w
25–15Me			w	w	s		s			
25–23		w	m	m	w	w	s	w	m	w
26–2Me			w			m	m			
27–2Me			m			s	m		m	
27–15Me			w			m				
28–2Me			w	w		m	w		m	
28–6OMe			w			w	w	s		w
28–15Me			w		w	s			w	
28–23		w	s	m	s	s	w	s	w	s
Chain-desosamine	(**1**)	(**2**)	(**1**)	(**2**)	**C1**$^+$–*Z*	**C2**$^+$–*Z*	**C2**$^+$–*E*	**C3**$^-$–*Z*	**C3**$^-$–*E*	**C4**$^-$–*Z*
26–5′Me			w	w				w	s[f]	w
27–5′Me			w					m[e]	w	
Desosamine-macrocycle		(**2**)	(**1**)	(**2**)	**D1**	**D2**	**D3**	**D4**		
1′–4Me	m	m	s	s	s	s	m	m		
1′–5	m	m	s	s	s	s	s	m		
1′–6Me			m	w	m	w	m	w		
1′–6OMe				w	w	w	m			
2′–4Me				s	w	w	m	w		
2′–5			m	w	w	w	m	m		
2′–6Me			m	w	m	m	w	m		
5′–4Me			w		w	w		m		
5′–5			m		m	m	w	w		
5′Me–5			w		w	m		m		
5′Me–6Me			m	w	m	m	m			
5′Me–6OMe				w	w	w		w		

[a]Some evident intra-unit contacts found for the different structures are not specified.
[b]2D ^{1}H NOESY: $\tau_m = 800$ ms, NOEs > 0; 2D ^{1}H NOESY map, $\tau_m = 150$ ms, in D_2O buffered solution (≈2 mM), pH 7.6, is empty.
[c]TRNOESY + ribosomes 0.8 μM, $\tau_m = 150$ ms, TRNOEs < 0 experiments in D_2O buffered solution (≈2 mM) at 293 K and pH 7.6.
[d]2–3 Å, s: strong, 3–4 Å, m: medium, 4–5 Å, w: weak.
[e]M1D1C3, S^-–*Z*.
[f]M2D2C3, S^-–*E*.

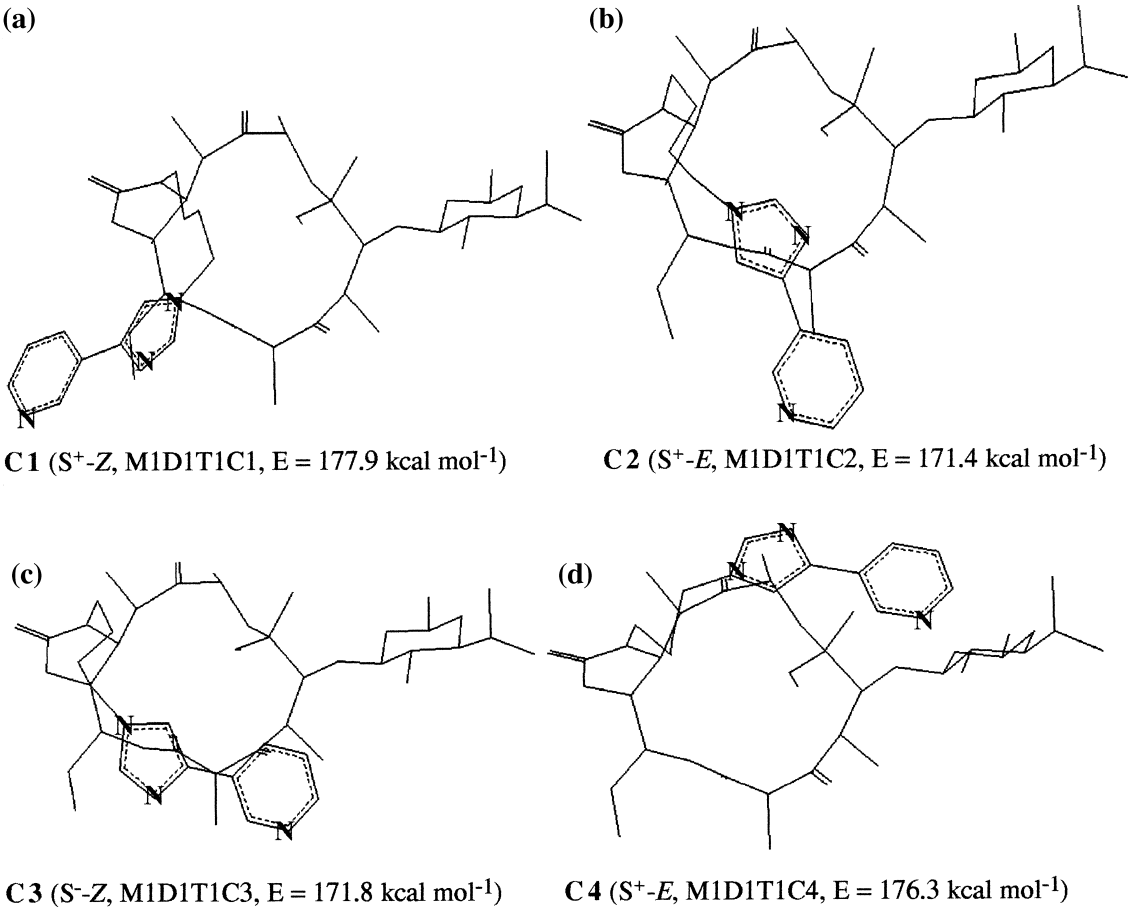

Figure 5. The four stacking conformers with the aromatic imidazolyl-pyridine chain: (a) above the carbonyl groups 16-CO (**C1**): the **C1** chain seems to be pushed back towards the left part of the macrocycle, in the C(11)–C(13) region; (b) above the carbonyl group: 1-CO (**C2**); (c) above the two carbonyl groups: 1-CO and 3-CO (**C3**); (d) above the 6-OMe group and the carbonyl group 9-CO (**C4**).

imidazol-pyridine protons and the macrocycle showing probably a libration of the end of the chain. Concerning the desosamine unit, few contacts with macrocycle are observed for HMR 3647 and RU 72366 molecules, attesting to some mobility. The sugar-lactone NOEs from H(1′), [1′]4-Me, [1′]5 as the set of $^{3}J_{^{13}C-^{1}H}$ coupling constants (Table 3) suggest that the position of this unit corresponds to a major perpendicular orientation '**D1**' or '**D2**'. The NOEs [1′]6-OMe, [2′]5 and [2′]6-Me characteristic of '**D3**' and the connectivities [5′]4-Me and [5′-Me]4-Me indicating an orientation '**D4**' of the desosamine unit are missing for HMR 3647 and RU 72366.

The missing NOEs in no way affect the conclusion that although more than one conformer is present in water, one conformer dominates. The crystal structure **1** and the dominant conformer of **1** and **2** in water have the same or very similar conformation.

Carbon-13 spin-lattice relaxation times (T_1). T_1 values were used to probe the mobility of the protonated carbons in HMR 3647 and RU 72366. Information about the structural flexibility of these compounds can be obtained experimentally from the T_1 relaxation times of the carbon resonances as the NT_1 values (N = number of attached protons, T_1 = longitudinal relaxation time) correlate directly with the molecular mobility.[41]

The methyl Me(2), Me(4), Me(6), OMe(6) and the methylene CH_2(7) groups of HMR 3647 molecule have shorter NT_1 values ($\approx -30\%$) compared to demethylated derivative (RU 72366) (Fig. 6). In HMR 3647, the mobility is reduced on one side, C(2)–C(7) of the macrocyclic ring, in agreement with a major presence of the **M1** conformer and according to the observed $^{3}J_{4,5}$ values, while the longer NT_1 values ($\approx +20\%$) of Me(8), Me(10), Me(12) and Me(15) of HMR 3647 molecule suggested an increased mobility of the opposite side, C(8)–C(15). Namely, the folding of the C(3)–C(5) portion of the major lactone ring **M1** in HMR 3647 moves Me(4) to a more outside ring position, but forces it closer to the Me(2). The Me(4) is thus pushed into a more sterically congested environment. This reorganisation results after removal of cladinose sugar in ketolides. The existence of hydrogen bonding from NH_3^+ observed by molecular modelling calculations also contributes to restrict desosamine sugar rotation in RU 72366. In the same time, the [ΔNT_1] values are markedly lower in RU 72366 than in HMR 3647 (20%). The NT_1 values of the flexible side chain were slightly longer in HMR 3647

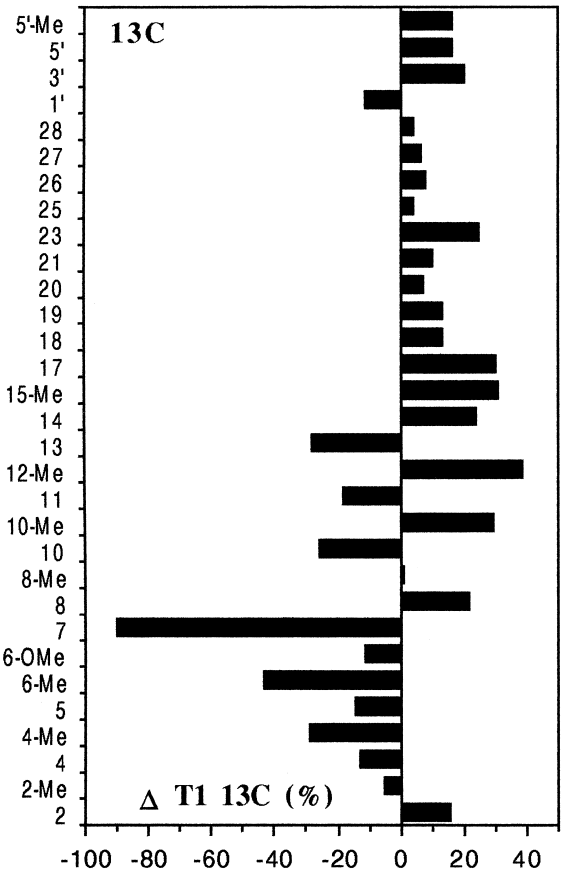

Figure 6. Differences (%) in experimental ^{13}C NMR relaxation times (T_1) in D_2O solution between HMR 3647 (**1**) and RU 72366 (**2**) for macrocycle ring, desosamine sugar and chain unit.

than in the RU 72366 derivative, in good agreement with the absence of NOEs between the chain and the erythronolide for HMR 3647.

Molecular modelling. We performed computational chemical studies (molecular dynamics and molecular mechanics calculations) starting with the X-ray crystal structure of HMR 3647 supplied by Hoechst Marion Roussel laboratories since the data are not available through the Cambridge Crystallographic Database (Fig. 2). The crystal structure of HMR 3647 presents different characteristics as shown by X-ray analysis (Fig. 2a) (crystal data S^- obtained in isopropyl ether and acetone: tetragonal crystal; $a=11.66$ Å, $b=11.66$ Å, $c=63.93$ Å; space group $P4_12_12_1$; $R=4.7$). The minimised structure of HMR 3647 (Fig. 2b) obtained by X-ray diffraction revealed an interesting feature of the erythronolide ring (M1T1) with the desosamine sugar (**D1**) oriented perpendicular to the macrocyclic lactone ring (Fig. 4c). This minimised (S^-–Z) structure is referred to S^- and to S–Z, respectively, because the last rotor corresponding to the alkyl part of the chain, the C(20)–N(20) dihedral angle, is g^- (S^-) and two nitrogen atoms corresponding to the imidazolyl-pyridine part of the chain, the C(23)–C(28) torsion angle are *eclipsed* (S–Z) (Fig. 3). The aromatic imidazolyl-pyridine chain overlaps the C(13)–C(15) region of the macrocycle displaying typical (**C1**) stacking conformation (Fig. 5).

The desosamine sugar was modified to include a protonated amino group at the 3′-position, then the charges were recalculated[42] in the CVFF force field.[43] The above calculations presumed the default value of $\epsilon=4r$ for the local dielectric constant, a reasonable analogy for the solvent. Molecular dynamics were performed from different initial structures with distance constraints based on the observed NOE data. The constraints corresponding to NOE inter-units were introduced in the form of quadratic potential with 2 Å lower limit and 5 Å upper limit.

The final structures obtained after several such calculations (Fig. 7a) were examined for the overall energetic favourability and compared with the structure derived from the NMR data (Tables 2 and 3). Structures found to have more energy up to 10 kcal mol^{-1} will be representative of very hindered intermediates. The 27 lowest energy conformations resulting from this study are listed in Table 4 and these conformers will be referred to from here on by the names in this table.

Molecular dynamics. To simulate the molecular motions in solution, different protocols of molecular dynamics have been used. In order to find suitable parameters (charge values, times, temperature) we varied them systematically. As can be seen in Table 4, five conformational families ($\mathbf{S_I}$–$\mathbf{S_V}$) were found. MD simulation was performed from the four different initial structures (S^+–Z and S^+–E, S^-–Z and S^-–E) with distance constraints based on the observed NOE data and the results are reported in Table 5 and illustrated in Figure 7a. The global minimum was found in the very first trial and the lowest energy conformations (Fig. 7b) were found to be **S2**$^+$–Z M1D1T1C2 and **S3**$^-$–Z M1D1T1C3. The g^+ (S^+) conformation favoured the stacking of the imidazol unit with CO(1) in the **C2** chain conformation. Conversely, the g^- (S^-) conformation led to the stacking of the imidazol and the pyridine units with, respectively, both carbonyls CO(1) and CO(3) in the **C3** conformation.

Molecules HMR of lowest energies generated during 800 ps dynamics protocol with distance constraints (Fig. 7b) are mainly of M1D1T1 conformation, involving both imidazolyl-pyridine chain conformations, '**C2**' (50%) when starting from S^+ structures (the chain is directed towards the 2-Me) and '**C3**' (45%) conformer when starting from S^- structures (the chain is stabilised by the stacking of both carbonyls, 1-CO and 3-CO). A $S1^+$–E M1D3T1C2 structure of higher energy ($\Delta E=+4.8$ kcal mol^{-1}) exhibits a coplanar desosamine conformation, named '**D3**', which was allowed when '**C2**' position of the chain disrupts the stacking which occurred between CO(3) and pyridine ring.

RU72366 presented essentially M1D1T1C2 (77%) conformation, $S2^+$–Z predominant. The S^-–Z structure was not stable during the 300 K MD simulation performed with distances constraints based on the NOE data and an interconversion to S^+–Z was observed. The minor conformation M1D3T1C2 corresponds to a structure $S1^+$–Z of 'higher energy' (4.7 kcal above the

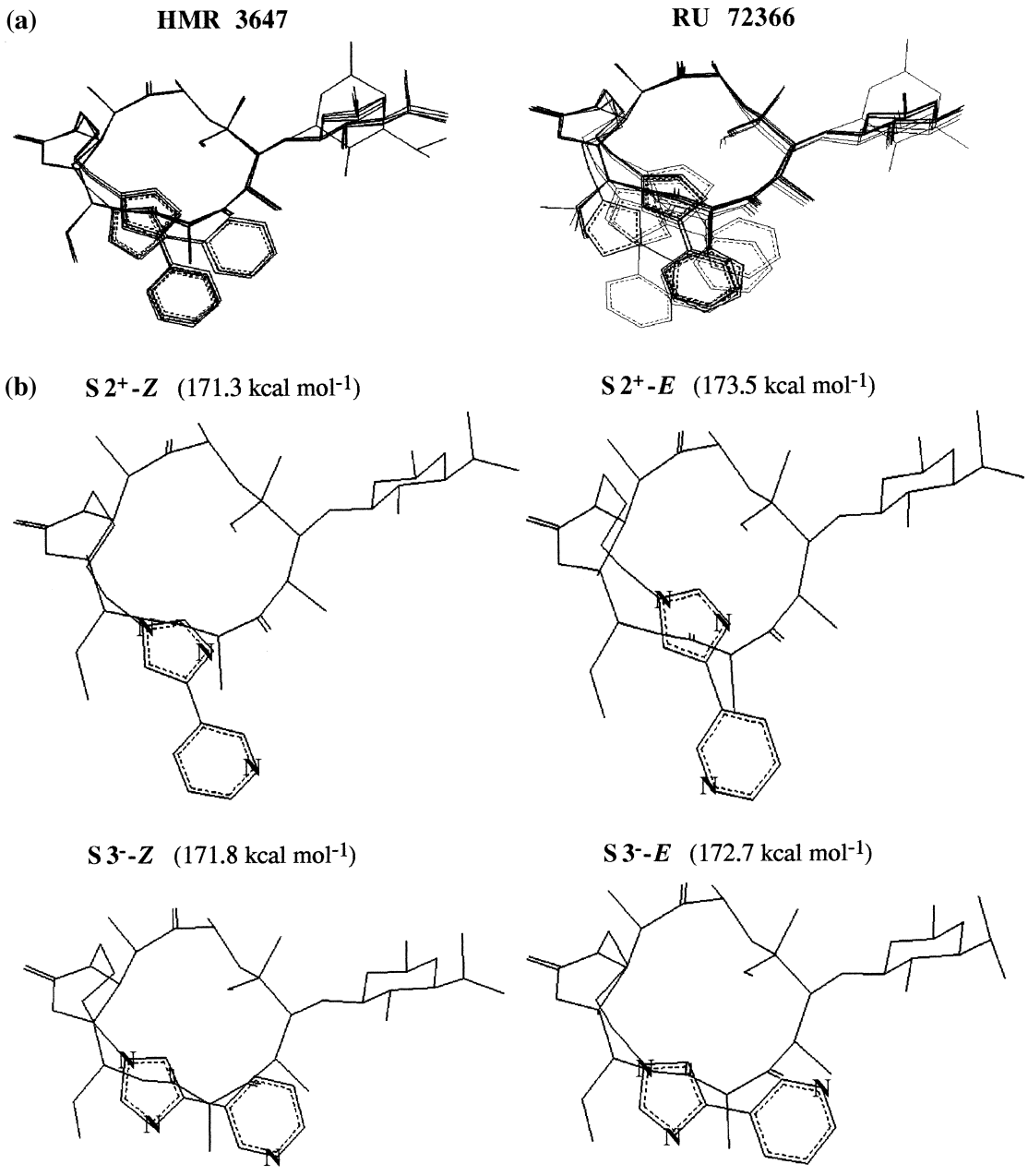

Figure 7. (a) Superimposition of the lowest energy structures (in solution) generated from NOE data for HMR 3647 (**1**) and for RU 72366 (**2**). (b) The four lowest energy HMR 3647 conformations: in $\mathbf{S2}^{+}$–***Z*** ($E = 171.3$ kcal mol^{-1}) and $\mathbf{S2}^{+}$–***E*** ($E = 171.4$ kcal mol^{-1}), the **C2**(+) conformation of the chain is indicative of the aromatic imidazol ring stacked above the carbonyl group: CO(1), while in $\mathbf{S3}^{-}$–***Z*** ($E = 171.8$ kcal mol^{-1}) and $\mathbf{S3}^{-}$–***E*** ($E = 172.7$ kcal mol^{-1}), the **C3**(−) conformation of the chain is indicative of the aromatic imidazolyl-pyridine stacked above CO(1) and CO(3), stopped at the right hand side by the OMe(6) group and finally ending up above the contact region between the sugar unit and the macrocycle.

minimum). The S^{+} conformation gives rise to a free rotation of the ethyl group which can take up two positions, mainly **T1** and **T2**, M1D1T2C2.

Two main differences between the two ketolides, HMR 3647 and RU 72366, appeared. Firstly, the M1D1 structures from MD are more stable by 5 kcal for HMR 3647 and by 8.5 kcal for RU 72366 than the corresponding M2D2 ones. Then, M2D2 conformations can be favoured for HMR 3647 if the necessary activation energy for this observed transitional event ('**M1**↔**M2**') was attained in solution. Secondly, the major structure of HMR 3647, $S3^{-}$–*Z*, was not stable in RU 72366 solution even during protocol without raising of the temperature (300 K). An interconversion was observed only for RU 72366, the S^{-}–*Z* conformer leading to the S^{+}–*Z* one. The minimum energy structures of the demethylated derivative always present the following hydrogen bonds, 3′-NH_2^{+}///OH(2′) and 2′-OH///O(5).

It is thus concluded, from NMR and MD data, that HMR 3647 exists in aqueous solution as the major conformers (Fig. 7), M1D1T1C2 ($S2^{+}$–*Z* and $S2^{+}$–*E*) and M1D1T1C3 ($S3^{-}$–*Z* and $S3^{-}$–*E*). The analogue RU 72366 presents the similar M1D1T1C2 ($S2^{+}$–*Z* and

Table 4. Energy computed for structure families of HMR 3647 and RU 72366 represented by 27 low energy conformations

			HMR 3647				RU 72366			
Family	Structures[a]	Conformation	S^+–Z	S^+–E	S^-–Z	S^-–E	S^+–Z	S^+–E	S^-–Z	S^-–E
S_I	S1	M1D1T1C1	177.9					163.7	160.5	161.5
	S2	M1D1T1C2	171.3	173.5	173.6	173.7	156.8	159.0		158.9
	S3	M1D1T1C3			171.8	172.7			157.3	158.2
	S4	M1D1T1C4			176.4	177.2	161.7		160.5	160.6
	S5	M1D1T2C1					160.9	161.0	163.2	163.3
	S6	M1D1T2C2	173.1	175.0	174.8	174.8	158.6	160.5		
	S7	M1D1T2C3			173.3	174.6			158.6	160.1
	S8	M1D1T2C4					163.2		161.5	161.7
	S9	M1D1T3C2	175.2					162.7		
	S10	M1D1T3C3			176.8					
S_{II}	S11	M1D3T1C2		176.1			161.5	161.6		
	S12	M1D3T1C3			174.2	175.3			160.1	160.8
	S13	M1D3T1C4					163.4			
	S14	M1D3T2C2		177.8						
	S15	M1D3T2C3			175.6	177.2				162.8
S_{III}	S16	M1D4T1C2	175.3	177.3			163.3	162.8		
	S17	M1D4T1C3			175.2				160.6	161.6
	S18	M1D4T1C4					163.5		163.9	
	S19	M1D4T2C1						161.0		
	S20	M1D4T2C2					164.6			
S_{IV}	S21	M2D2T1C2	176.3				165.5			
	S22	M2D2T1C3				176.7				
	S23	M2D2T1C4							165.2	164.1
	S24	M2D2T2C2	176.8					174.7		
	S25	M2D2T2C3			177.6				161.1	162.0
S_V	S26	M2D4T1C3							160.7	
	S27	M2D4T2C3							162.4	

[a]The structures of high energy were exceptionally generated by a protocol using temperature jumps at 600 K and starting from one S^- or S^+ (S–Z or S–E) structure built using the INSIGHT II builder module. Therefore, they are never generated during 1200 ps, at 300 K. At 300 K, during 200 ps an interconversion was observed from $S^-(Z)$ to $S^+(Z)$ but no interconversion from S–Z to S–E structures.

$S2^+$–E) major conformers, but it cannot adopt the $S3^-$–Z conformation. The other minor conformations are present to a lesser extent in aqueous solution.

Structural characteristics of the ligands bound to the bacterial ribosome

Taking advantage of the exchange between bound and free macrolide antibiotics, we have developed a study of ketolide–ribosome interactions of HMR 3647 and RU 72366 to *Escherichia coli* ribosomes, using two-dimensional transferred nuclear Overhauser effect spectroscopy (TRNOESY).[16,18,25] The information present in TRNOE analysis focuses on a plausible conformation essential for the antibacterial action when binding to the bacterial ribosome. We have previously shown that the major conformer of the ketolide, RU 004, present in solution binds to bacterial ribosomes, specifically to the 50S subunit, in a fast exchange process on the NMR timescale.[9] Room temperature seems better for fast exchange upon complex formation and leads to optimal conditions for TRNOESY experiment. The experiments were performed with a large excess of ligand (5000 equivalents with respect to the ribosomes), with potassium phosphate buffer 50 mM, KCl 200 mM and $MgCl_2$ 10 mM at apparent physiological pH 7.6. As the ketolide exchanges very rapidly between the free and the bound state, only the TRNOE-derived distances are suited to calculate the ribosome-bound structures of HMR 3647 and RU 72366.

Transferred nuclear Overhauser enhancement experiments. Upon the addition of ribosomes, the resonances of HMR 3647 showed a pronounced line broadening, indicating its interaction with the ribosomes. Interestingly, the lines corresponding to RU 72366 showed the same effect. In the TRNOESY experiment, a high number of negative cross peaks demonstrated the interaction of HMR 3647 and RU 72366 with ribosomes. TRNOESY spectra were recorded with different mixing times. The intensity of the few positive cross peaks in the NOESY spectrum ($\tau_m = 800$ ms) was estimated to be weak enough for neglecting the cross-relaxation of the free ketolide in the interpretation of TRNOESY spectra recorded at 50, 100 and 150 ms. Internuclear distance information was obtained from TRNOE data by the evaluation of cross-peak volumes, since the ratio of two intermolecular distances can be related to these volumes.[44,45] Interproton distances were attributed to three categories, weak (w), medium (m), and strong (s) (Table 3).

The intra-macrocycle TRNOEs. The structures representing the bound state of the ketolides, HMR 3647 and RU 72366, presented many more new intra-erythronolide TRNOEs (Table 3). The identification of the negative cross peaks revealed that most of them were due to TRNOE effects between protons of the **M1** conformer as the other new intra-erythronolide TRNOEs {13}6OMe, {15Me}Me(2) were specific for a **T1** ethyl group conformation. Only a few negative cross peaks

Table 5. Simulations at 300 K with dielectric constant $\epsilon = 4\ r$ starting from four S^+–Z, S^+–E, S^-–Z, S^-–E conformations with distances constraints based on the NMR data

			Starting **S** conformations (frequency)									
			HMR 3647					RU 72366				
MD[a] with distances constraints based on the observed NOEs data[b]			S^+–Z	S^+–E	S^-–Z	S^-–E	(%)	S^+–Z	S^+–E	S^-–Z	S^-–E	(%)
S_I	S2	M1D1T1C2	192	168	18	21	50	179	158	142[c]	132	76.4
	S3	M1D1T1C3			181	179	45				9	1.1
	S6	M1D1T2C2							42	51[c]	4	12.1
	S9	M1D1T3C2									30	3.8
	S10	M1D1T3C3									20	2.5
S_{II}	S11	M1D3T1C2	7	31			4.7	20		3[c]		2.9
	S13	M1D3T1C4								4[c]		0.5
S_{III}	S16	M1D4T1C2	1		1		0.2	1				0.1
S_{IV}	S21	M2D2T1C2		1			0.1					
	S22	M2D2T1C3									2	0.2
	S25	M2D2T2C3									3	0.4
MD[a] with distance constraints based on the observed TRNOE data MD with 45 distance constraints			S^+–Z	S^+–E	S^-–Z	S^-–E	(%)	S^+–Z	S^+–E	S^-–Z	S^-–E	(%)
S_I	S2	M1D1T1C2						198	3			25
	S3	M1D1T1C3			80		7			200	59	32
S_{III}	S16	M1D4T1C2		8				2				
	S17	M1D4T1C3				8						
S_{IV}	S21	M2D2T1C2		292			24		197			25
	S22	M2D2T1C3	292		220	292	67				141	18
	S26	M2D4T1C3	8									
MD with 25 distances constraints			S^+–Z	S^+–E	S^-–Z	S^-–E	(%)	S^+–Z	S^+–E	S^-–Z	S^-–E	(%)
S_I	S2	M1D1T1C2	295	266			46	300	299	3	11	51
	S3	M1D1T1C3			296	299	50			290	282	48
	S4	M1D1T1C4									2	
	S7	M1D1T2C3				1					1	
S_{III}	S16	M1D4T1C2	4	7					1			
	S17	M1D4T1C3								2	2	
S_{IV}	S21	M2D2T1C2	1	37			3					
	S22	M2D2T1C3			4					5	2	

[a]Each column represents one simulation and the frequency is the number of times each conformation was found.
[b]Calculations were performed with distance constraints based on the observed NOE data.
[c]Structures S^+–Z are generated from the starting structures S^-–Z only for RU 7236. At 300 K the interconversion from S^-–Z to S^+–Z structures was observed. Therefore, no interconversion was observed from S–Z to S–E.

corresponding to the **M2** isomer were present such as the {11}4 connectivity which appeared in the bound structure ($d_{11,4} = 4.8$ Å for **M1** and 3.2 Å for **M2**).

The imidazolyl-pyridine chain TRNOEs. For HMR 3647 and RU 72366, the TRNOEs observed at 150 ms ({21 and 23}2Me, 15Me, 6OMe) demonstrated the stacking which occurred between CO(1) and imidazol ring since the two imidazol protons, H(21) and H(23), are located above Me(2) and equidistant from Me(15) and OMe(6). In the same way, there was a stacking between CO(3) and pyridine ring since the two pyridine protons, H(25) and H(28), are also located above Me(2) and equidistant from Me(15) and OMe(6). The position of the aromatic imidazolyl-pyridine chain in the bound structure seems to be pushed back towards the right part of the macrocycle, in the C(1)–C(3) region. The imidazolyl-pyridine chain in the bound structures was held towards CO(1) and CO(3) between Me(15), Me(2) and OMe(6). Finally, the inter desosamine-chain TRNOEs {5′Me}26 and 27 show that the end of the chain was close to the contact region between the macrocycle and the sugars unit (**C3** conformation). These inter macrocycle–aromatic chain TRNOEs (Fig. 8) were only present in the bound state since contacts of the chain with the erythronolide are either non-existent in the free HMR 3647 or only concerned the alkyl part of the chain in the free RU 72366.

The spatial proximities observed from imidazol protons, H(21) and H(23), and from pyridine protons, H(25) and H(28), with the macrocycle as the connectivities between the protons, H(26), H(27) with the sugar ring, allow us to conclude that the bound structure is preferentially referred to one **C3** chain in a S^-–Z structure (presence of a strong {23}28 TRNOE).

The inter-macrocycle–desosamine TRNOEs. As evidence from the constraints of the different TRNOEs observed in buffered D_2O, the relative rigidity of the sugar unit in ketolide–ribosome complex seems to be confirmed. Two desosamine–lactone NOEs {5}1′ and {4Me}1′ are observed as well for free as for bound structures. These two interactions and the new spatial proximities {1′}Me(6), {2′}Me(6), {5′}Me(4), {5′}5, {5′Me}5 and {5′Me}Me(6) present in bound HMR 3647 structure are

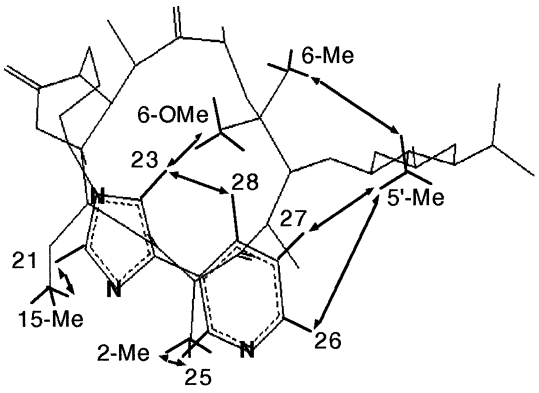

Figure 8. Some characteristic TRNOEs for the bound HMR 3647 (**1**) structure.

exactly those expected if the desosamine sugar ring is oriented approximately perpendicular to the macrocycle lactone ring (**D1** or **D2** conformation). The desosamine ring adopts a rather similar orientation for the two bound HMR 3647 and RU 72366 conformations. However, some differences between the two bound structures appeared in the macrocycle–desosamine interactions. Firstly, a new {1′}OMe(6) connectivity characteristic of the '**D3**' conformation was only observed for RU 72366. Secondly, three TRNOEs {5′}Me(4), {5′}5, {5′Me}5 expected for '**D1** or **D2**' and present in HMR 3647 were missing in '**D3**' conformation and in RU 72366 bound structure.

MD simulations with distance constraints. From the TRNOE-distance constraints (Fig. 8), the bound conformation was calculated, thus we were able to determine a family of very well resolved conformations, which could indicate the specific structural requirements of the weak binding receptor. The distances defined from the relative TRNOESY cross-peak intensities were set as follows: 2–3 Å (s), 3–4 Å (m) and 4–5 Å (w). Distances including methyl protons were referred to pseudo-atom, located to the centre of the three methyl protons.[46]

Set of calculations. To calculate the bound conformations, 45 TRNOE-derived distances were used (Table 5). 1200 structures were generated during this protocol (Fig. 9a), after four dynamics (300 ps MD run at 300 K) starting from (S^+–Z, S^+–E) and (S^-–Z, S^-–E) structures. The quality of the resulting structures was evaluated by the average distance error $(1/N\Sigma[d_{set}(i)–d_{model}(i)]$ where N is the number of constraints and d_{set} and d_{model} correspond to the distance from the constraint set and to the distance calculated from the generated conformation, respectively). The average distance error for constraints involving backbone atoms varied from 0.4 to 0.6 in the retained structures. These violations appeared to be minor, mainly when the residues, imidazolyl-pyridine chain presented the **C3**$^-$–Z chain conformation, and macrocycle the M1D1 and M2D2 conformations. Then, two macrocycle conformations (**M1** and **M2**) may coexist while the free HMR molecules generated with NOE distance constraints were

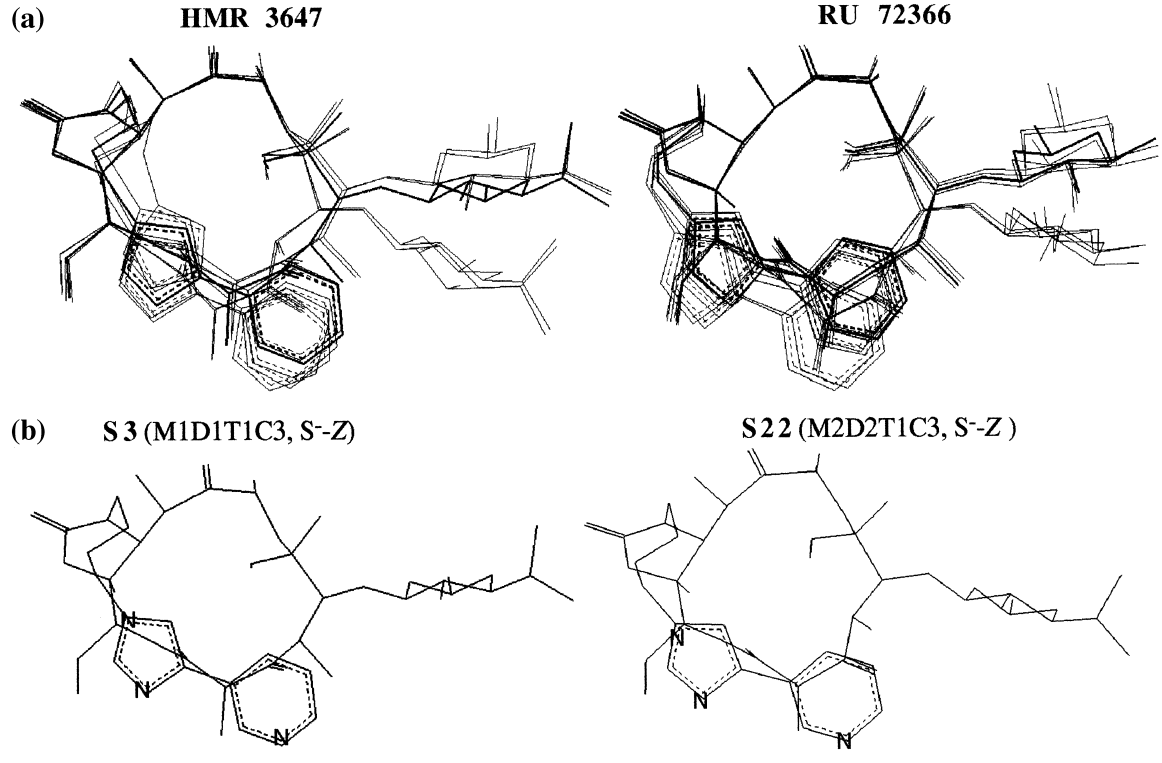

Figure 9. (a) Superimposition of the lowest energy structures (bound to bacterial ribosomes) generated from TRNOEs data (with 45 TRNOESY distance constraints) for HMR 3647 (**1**) and for RU 72366 (**2**). (b) Two structures represent the bound state for the two drugs, **S3**$^-$–***Z*** (M1D1T1C3) for **1** (173.6 kcal mol^{-1}) and **2** (160.6 kcal mol^{-1}) and **S22**$^-$–***Z*** (M2D2T1C3) for **1** (175.3 kcal mol^{-1}) and **2** (164.6 kcal mol^{-1}).

mainly of M1D1 conformation. The best conformations found to be consistent with our input data were retained, **S3**$^{-}$–*Z* M1D1T1C3, one of the free predominant conformation and **S22**$^{-}$–*Z* M2D2T1C3, structure predominantly generated (Fig. 9b). When MD runs were performed using the same four initial structures but with a limited group of 25 constraints (Table 5), selected as they never present violations in any generated structures, the conformations M2D2 were less favoured, statistically. The free major conformations (**S3**$^{-}$–*Z* M1D1T1C3 and **S2**$^{+}$–*Z* M1D1T1C2) were now predominantly generated while the **S22**$^{-}$–*Z* M2D2T1C3 structure corresponded now to the minor ones.

When TRNOESY data were applied to the structures of the drugs and minimised, HMR 3647 and RU 72366 gave rise to the low energy structures shown in Figure 9b. Two types of structures representing the bound state show great similarity for the two drugs, **S3**$^{-}$ (M1D1T1C3) and **S22**$^{-}$ (M2D2T1C3). The **S3**$^{-}$ (M1D1T1C3) structure given represents one of two minima (**S3** and **S2**) generated from free HMR 3647 MD simulation (Fig. 7). The other **S22**$^{-}$ (M2D2T1C3) structure shows a great distortion in the macrolide ring from the free state structures.

The possible alternatives are that either (i) HMR 3647 and RU 72366 bind directly to the receptor with their major conformation in solution and M1D1T1 (**C2**, **C3**) isomers are the active structures or (ii) conformational changes M2D2 is involved and M2D2T1 (**C2**, **C3**) isomers interact with the receptor in multisteps kinetics. The potencies of the ketolide interactions with the ribosome binding site should be at least partially dependent on the relative abundances of each of the ketolide conformations. The biological activity of ketolide antibiotics depends on many factors, and these may include their conformation in solution.

It is clear that, in the ketolides, the free space liberated by the cladinose confers to the 4-methyl group, the 5-desosamine sugar and the pyridine nucleus of the alkyl-aryl side chain more conformational freedom. This is demonstrated by the slight shifting of the **D2** desosamine toward the unoccupied cladinose area, or by the 4-methyl group moving out in the 3-keto area in the **M1** macrocycle or by the overlapping of the macrolactone ring by the **C3** stacking chain conformation which allow the nitrogen of the aromatic pyridine nucleus to interact in terms of attractive potential with the 3-CO carbonyl group. These modifications may be of importance for the ketolide mode of action. At the same time the south part of the macrolactone ring becomes more accessible to additional interactions.

Bound conformation. From these experiments, the **S3**$^{-}$–*Z* M1D1T1C3 and **S22**$^{-}$–*Z* M2D2T1C3 conformations (Fig. 9b) appear to be the plausible bound structures relative to this weak specific binding to the bacterial ribosome. Indeed, the structures representing the bound state of the drug HMR 3647 shows conformational homology with the bound conformation of RU 72366, after superimposition (Fig. 10a). Previous studies[9] of a

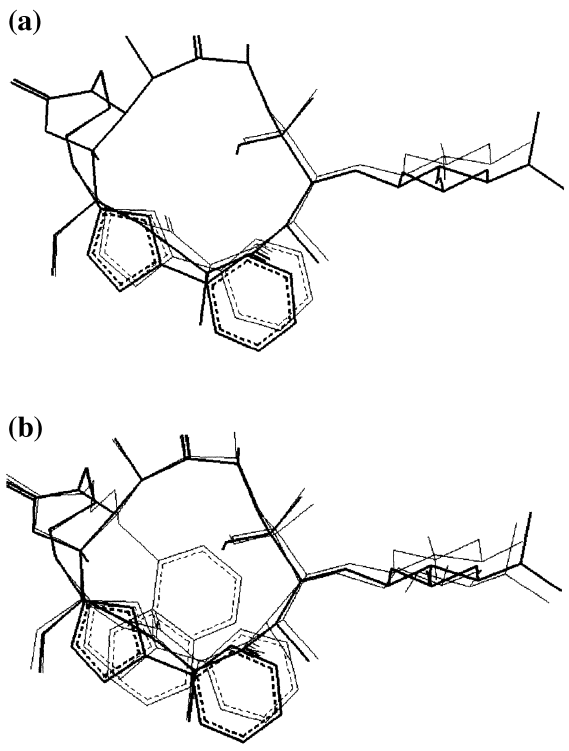

Figure 10. (a) Superimposition of **S3**$^{-}$–***Z*** (M1D1T1C3) conformations generated by MD and TRNOESY derived structures, weakly bound to bacterial ribosomes for HMR 3647 (**1**) and RU 72366 (**2**). Quality of superimposition of all the atoms was evaluated by mean square (rms) deviation between the atoms constituting the HMR 3647 (**1**) bound conformer in bold and the corresponding atoms in the **S3** conformation, for **2** (rms, 0.011 Å). (b) Superimposition of ketolide bound conformations: **S3**$^{-}$–***Z*** (M1D1T1C3) for HMR 3647 (**1**) in bold and RU 72366 (**2**) and TRNOESY derived structure, weakly bound to bacterial ribosomes for RU 004 (rms, 0.1363 Å).

ketolide derivative, RU 004, have postulated an hypothesis about the conformational requirement of ketolide ribosome target that it was interesting to strengthen. Considering the interaction between ketolide and ribosome, the three functional groups, namely the two carbonyls CO(1) and CO(3) and the amino group of the desosamine moiety $NH^{+}(3')$, in addition to the Me(15) group, should be adequately arranged to favourably fit into the receptor. After superimposition (Fig. 10b), only the HMR 3647 **S3**$^{-}$–*Z* M1D1T1C3 bound structure was most similar to this earlier drug in the series (RU 004). The conformation of the 14-lactone ring is characterized by the 'up' position of the two carbonyl groups CO(1) and CO(3) which are maintained by stacking with the imidazolyl-pyridine chain and the outward folding of the 4-methyl group and the desosamine moiety. The imidazolyl-pyridine chain should play a role in arranging the spatial position of the additional nitrogen and the aromatic nucleus in the ketolide molecules. It was demonstrated earlier that the introduction of a supplementary amino group in the macrolide skeleton was beneficial for their activity.[47] The introduction of an aryl-alkyl side chain resulted in a significant increase of activity against resistant strains. The aryl group as well as the length of the chain and finally introduction of additional nitrogens through the hydrazono function as well as the quinoline, the imidazol and the pyridine

nucleus, allowed us to obtain the desired profile of activity. The bound conformation was then evaluated to determine the conformation of the keto aglycone and the stereochemistry of the aryl-alkyl side chain, beneficial with regard to the overall spectrum.

Three main differences appear between the two ketolides HMR 3647 and RU 72366. It is to be noted that, firstly, the major conformation **S2**$^+$ (M1D1T1C2) of free RU 72366 (less active molecule) does not present the same structural analogy to the structure relevant to the receptor binding conformations (**S3**$^-$) while for HMR 3647, its free conformation in solution is mainly represented by the **S3**$^-$ one. Secondly, the **S3**$^-$ conformation of free RU 72366 (the plausible bound structure) was not stable during MD protocol. At 300 K, **S3**$^-$ was transformed into the **S2**$^+$ conformer from the beginning of the MD runs. Finally, if the **S22**$^-$ (M2D2T1C3) structure interacts with the ribosome, it seems more difficult for RU 72366 to reach a particular high free energy by a molecule for binding to the ribosome as the M1D1 structures are more stable by 5 kcal for HMR 3647 and by 8.5 kcal for RU 72366.

Binding surface. In general, a correlation between line broadening and involvement in binding is expected. Line broadening in NMR spectra may result from two distinct processes, equilibrium between states with different chemical shifts and slowing of molecular motion. Macrolides bind to ribosomes at an identical 'surface' of the drug molecule to erythromycin A, involving the C(13)–C(5) lactone region of the aglycone and both sugar rings.

Finally, a model of ketolide, HMR 3647, showing the hydrogen atom giving the most extensively broadened resonances is constructed (Fig. 11) using van der Waals' surfaces. The 'surface' of ketolides deduced from the variation in line broadening would be indicative of the relatively rigid part of the molecule. However it is not initially exact for the free molecules. The data corresponding to the C(4)–C(5) region are indicative of near-rigid rotation of these atoms in close proximity to the ribosome due either to a sterically hindered rotation or to specific inter-unit (ribosome–ketolide) bonds involving this region.

M1D1C3 and/or M2D2C3 conformations appear to be the plausible bound structures relative to this weak specific binding to the bacterial ribosome and the broadening observed in the C(10-Me)–C(12-Me)–C(15-Me)–O(14)–C(2-Me)–C(4-Me) region; C(23), C(1′), C(3′-N(Me)2) and C(5′-Me) may reflect proximity to a binding surface. These methyl substituents favour hydrophobic interaction between HMR 3647 and the ribosome.

The minimised structures derived from MD experiments will be compared to the ones suggested for macrolides (Fig. 12).[25,48,49] The better of the two structures M1D1C3 and M2D2C3 representing the bound state of the drugs (ketolides and macrolides) which really show conformational homology after superimposition (Fig. 12) was M2D2C3. Its C(2)–C(7) region is almost completely superimposable (Fig. 12b) while variation appears on the other side of the molecule. Because of the presence of a 3-keto function, the flexible right hand side of the macrocycle ring C(2)–C(4) of the major conformation '**M1′**' (H(4)–C(4)–C(5)–H(5), *trans*) exhibits some deviation from the 'folded-out' conformation (H(4)–C(4)–C(5)–H(5), *eclipsed*) found in erythromycin derivatives. This corresponds to an important variation between 14-membered macrolide and ketolide families as for both the desosamine sugar was found to be essentially perpendicular to the macrocycle (**D1** or **D2** conformer). Superimposition of the bound structures (Fig. 12) revealed one change that may be of importance for the ketolide mode of action, namely a stretching out of the desosamine sugar unit. This sugar moiety in HMR 3647 (16.2 Å) has moved by ca. 1.7 Å away from the C(15) region compared to erythromycin (14.5 Å). This distance was different with the *N*-demethylated RU 72366 derivative (13.4 Å) and it showed less antibacterial activity. A significant line broadening of the 3′-N(Me)2 and 5′-Me in desosamine unit may indicate a proximity of this residue in ketolide–ribosome complex as the line broadening affects the sugar units in other drugs. This may be due to the fact that 5-desosamine in both HMR 3647 and in erythromycin binds to the bacterial ribosome, but perhaps at different locations, or in a different way.

A significant line broadening affected the 12-, 15-methyl and the 2-, 4-methyl, positioned close to the CO(1) region. The broadening also involved some protons of the imidazolyl-pyridine chain, the group important for the appearance of activity in the ketolides. The broadening observed may reflect proximity of the chain to a binding surface involving an additional interaction of ketolide with ribosome. It can be postulated that the heteroaryl side chain also participates in positive interactions.

All these features may account for new binding interactions with the bacterial ribosomes. This study can explain some of the significant differences between HMR 3647 and the other antibiotics. Preliminary studies concerning the mechanism of action of ketolides that tends to demonstrate a second ribosomal binding site for the ketolides are in good agreement with this hypothesis.[50]

Conclusion

It was shown that the effect of the ketolide class was similar for HMR 3647 and RU 72366 compared to RU 004. The overall conformation of the macrolactone ring was not changed to a significant degree. The NMR data indicate that although more than one conformer is present in solution, two conformers (M1D1T1C2) and (M1D1T1C3) dominate. A combination of NMR spectroscopy and molecular modelling techniques showed that the major solution state macrocycle conformation is a CO(1), CO(3) 'up' type (**M1**). Two imidazolyl-pyridine chain conformers in solution are observed,

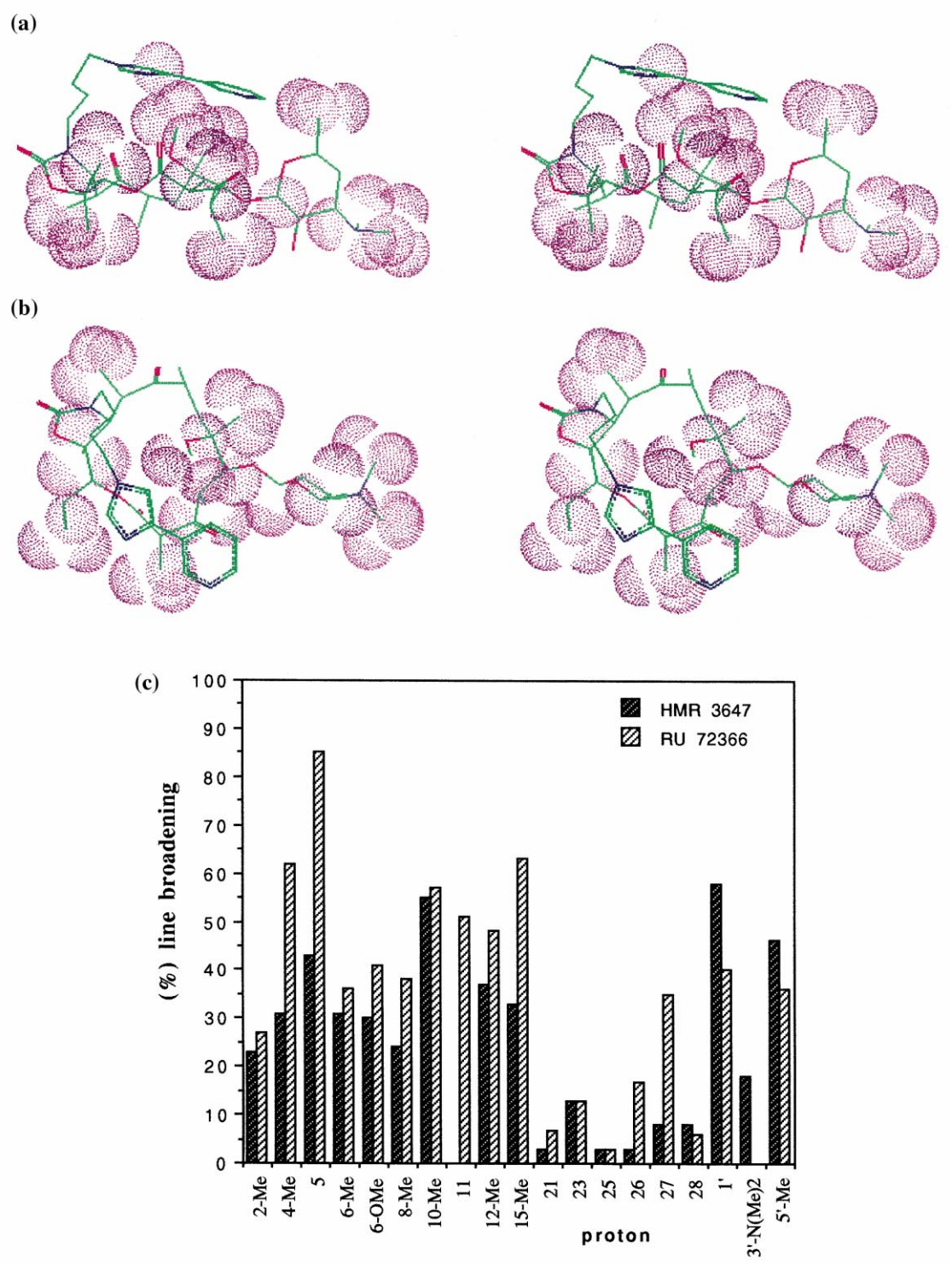

Figure 11. The van der Waals' surfaces are shown to indicate the atoms whose signals are broadened in presence of ribosomes, only for some protons of HMR 3647 (**1**) (1′-H, 10-Me, 5′-Me, 5-H, 12-Me, 15-Me, 6-Me, 4-Me, 6-OMe, 8-Me, 2-Me and 3′-N(Me)$_2$): (a) stereoviews of HMR 3647 (**1**) perpendicular to the macrocycle plane; (b) stereoviews of HMR 3647 (**1**) above the macrocycle plane; (c) differences in the observed line broadening in presence of ribosomes between HMR 3647 (**1**) and RU 72366 (**2**) for macrocycle ring, desosamine sugar and chain unit.

according to RU 72366 (**C2**$^+$) and to HMR 3647 (**C3**$^-$). These solution conformations might be relevant to the receptor binding conformations.

HMR 3647 displayed a significantly better response in TRNOE NMR experiments in agreement with a better overall antibiotic activity. In the HMR 3647 and RU 72366 bound structures (M1D1T1C3 and M2D2T1C3) in weak interaction with *E. coli* ribosomes, the data indicated that the imidazolyl-pyridine chain is anchored to the aglycone above the 3-keto 14-membered ring and the two carbonyls CO(1) and CO(3) are maintained 'up'

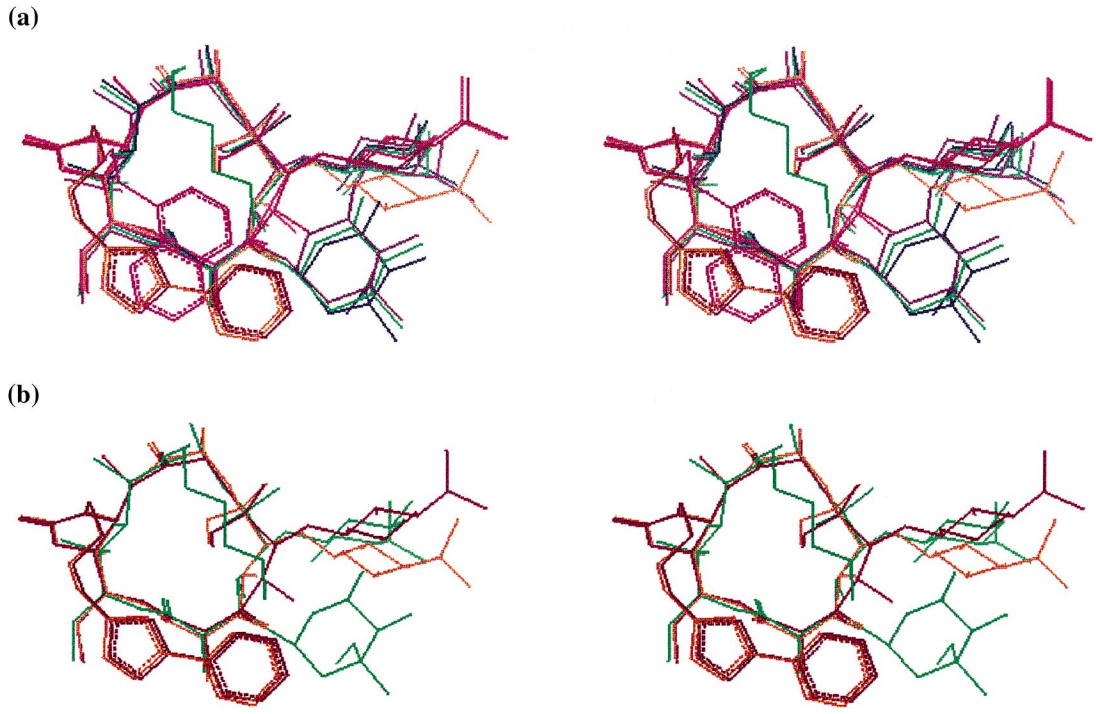

Figure 12. (a) Stereoviews of superimposition of ketolides: HMR 3647 (**1**), **S3**$^{-}$**–*Z*** (M1D1T1C3), red and **S22**$^{-}$**–*Z*** (M2D2T1C3), orange, RU 004, pink (rms, 0.0629 Å) and macrolides: roxithromycin, green (rms, 0.1931 Å), erythromycin, blue (rms, 0.2040 Å) and clarithromycin, purple (rms, 0.2042 Å) TRNOESY derived structures, weakly bound to bacterial ribosomes. (b) Stereoviews of superimposition of the TRNOE bound structures for the two drugs, roxithromycin, green and HMR 3647 (**1**), **S3**$^{-}$**–*Z*** (M1D1T1C3), red and **S22**$^{-}$**–*Z*** (M2D2T1C3), orange.

by stacking with the two aromatic nuclei. The bound structure gave predominantly the S^{-}–Z isomer but the corresponding one in the free RU 72366 analogue was not stable during the MD runs. The change of hydrophobicity on the target site, the transitional event ('**M1** ↔ **M2**') favoured in solution, the bound conformation **S3**$^{-}$–***Z*** favoured in the free state and a different shift of the desosamine sugar could explain why HMR 3647 molecule was more active against all major strains.

In the ribosome complex, the active molecules require similar orientation of one sugar, conformation perpendicular to the macrocycle ('**D1**' or '**D2**') compared to 14-macrolides, while the 4-methyl group and the C(3)–C(5) region may vary ('**M1**' or '**M2**'). Unlike RU 72366, the desosamine sugar moiety in HMR 3647 has moved by ca. 1.7 Å away from the C(15) region compared to 14-macrolides, in agreement with the bound RU 004 ketolide structure previously defined. Shifting of the sugar ring, modification of C(4)–C(5) bond angle, absence of steric hindrance in the C(3) area and additional implication of the imidazolyl-pyridine chain in the binding surface maintained by stacking with the 1,3-carbonyl group, all these properties may be of importance for the ketolides mode of action. These results can explain that ketolides exhibit higher affinity for weak ribosomal interaction than macrolides. Here also, TRNOE NMR experiments were proved to be efficient for the location and detection of the weak interactions due to ribosomal activity providing a relationship between conformation in interaction and activity.

Experimental

NMR spectroscopy

The samples HMR3647 and RU 72366 were dissolved in an aqueous NaD_2PO_4–Na_2DPO_4 buffer (0.05 M), with KCl (0.2 M) at apparent physiological pH 7.6 and it was possible to attain concentrations of 2 mM for ^{1}H experiments. Only for ^{13}C NMR spectra assignment, we had to previously dissolve RU 72366 in a minute amount of DMSO-d_6, to attain concentrations of 4 mM in D_2O buffer:DMSO-d_6 (97:3) solution. A crystal of $TSPD_4$, 3-(trimethylsilyl)[2,2,3,3-d_4] propionic acid, sodium salt, was used as internal reference for the proton shifts. The errors on the chemical shifts are 0.01 ppm for ^{1}H.

The experiments were run at 500 MHz for ^{1}H, at 293 K, on Bruker AMX 500 Spectrometers equipped with a Silicon Graphics workstation. A presaturation of the solvent was used for all the 1D and 2D ^{1}H experiments.

The 2D TOCSY spectra were recorded with data matrices of 2 K×256 points and processed using shifted sine bell squared window functions with zero filling in F_1 to 2 K×1 K. The mixing time was 70 ms. The ^{1}H–^{13}C correlation spectra were recorded at 125.77 MHz with data matrices of 2 K×256 and processed using sine squared window functions with zero filling to 2 K×1 K.

Three bond ^{13}C–^{1}H coupling constants were measured using a selective 2D INEPT experiment.[38] 64 experiments were carried out then data were zero-filled to 256

points in the F_1 dimension. In the F_2 dimension, data were acquired with 2048 points and no zero-filling was applied. Resolution enhancement by Gaussian transformation was realised in the F_1 dimension. The D_0 delay was initially set to a value of 3 μs and was increased by 17 ms between experiments.

The pH dependence of the *N*,*N*-dimethylamino, imidazol and pyridine protons as the 6-Me groups was studied with a 2×10^{-3} M D_2O solution at 293 K (pH = pD−0.4). This allows us to determine the three pK_a values by NMR, pK_{a1} = 8.7 for **1** and 8.1 for **2** (dimethylamine), pK_{a2} = 4.8 (imidazol) and pK_{a3} = 2.1 (pyridine), for **1** and **2**.

The 2D phase-sensitive ^{1}H NOESY experiments were performed using States-TPPI method with different mixing times from 400 to 1000 ms. FIDs were acquired over 5555 Hz into a 2-K data block for 256 incremental values of the evolution time and the relaxation delay of 2 s.

Transferred NOE effects from macrolide–ribosome interactions could be observed with a 5000 ligand/ribosome ratio. Microdialysis on Millipore membrane filters MF-type with 0.025 μm pore size was carried out beforehand with D_2O phosphate buffered solution for NMR to remove TRIS impurities present during ribosome isolation. A concentration of 0.4 μM of *E. coli* MRE 600 strain 70S ribosomes is appropriate because it gives a significant increase of the line width of HMR 3647 and RU 72366. The 2D phase-sensitive using States-TPPI method ^{1}H TRNOESY experiments in 2 mM D_2O buffered solution were performed using a mixing time of 50, 100 and 150 ms. FIDs were acquired (64 scans) over 5555 Hz into a 2-K data block for 256 incremental values of the evolution time and a relaxation delay of 2 s. Water suppression was performed by a low power transmitter pulse of presaturation (70 dB) during relaxation delay and mixing time. One half-sinusoid (5% truncated) shape homospoil gradient of 10 G cm^{-1} was used during mixing time.

Molecular modelling

The calculations were run on a Silicon-Graphics computer using the CVFF Force field from Dauber-Osguthorpe and Hagler[43] of Biosym software 'INSIGHT II' and 'DISCOVER'.

HMR 3647 and RU 72366 structures were built from the crystallographic coordinates of the solid HMR 3647 as a starting point. Their atomic potentials and charges were recalculated using the built-in algorithm of the program.[51] The starting structures were first minimised using 100 steps of the 'Steepest Descent' algorithm and then the 'Conjugate Gradients' algorithm until a convergence of 0.1 kcal mol^{-1} was reached. For the Molecular Dynamics calculations, the trajectories were calculated by means of the Verlet Algorithm used in the force field of DISCOVER. The system was then equilibrated over a period of 6 ps to reach a temperature of 300 K by coupling it to a thermal bath.[52] Subsequently, HMR 3647 and RU 72366 (S^+) were modelled and it did not appear to be inherently unstable. These data indicate the presence of a kinetic barrier to isomerisation S^-, S^+.

The dynamics were run for 50 ps (variable temperature) or 200 and 300 ps (constant temperature), the trajectory was sampled by minimising and storing the structure every picosecond. The 27 final conformers found with lowest energies were then further minimised to a gradient less than 0.01 kcal/mol to obtain their energies at higher accuracy. Conformational similarities were evaluated by calculating the RMS of deviation between heavy atoms for each possible pair of the different structures.

The lowest energy-minimised constrained structure extracted from simulations was compared with the bound ligands for ketolide RU 004 and 14-membered macrolides, using a superimposition procedure.

Ribosome preparation

The ribosomes were prepared at Hoechst Marion Roussel as described[53] by a tangential ultrafiltration technique. The ribosomal purity is given by one unity A_{260} (absorption at 260 nM) which corresponds to 24 pmol mL^{-1} of 70S ribosomes.

Acknowledgement

This work was supported by grants from Hoechst Marion Roussel (Romainville Research, Medicinal Chemistry).

References

1. Denis, A.; Agouridas, C.; Auger, J. M.; Benedetti, Y.; Bonnefoy, A.; Bretin, F.; Chantot, J. F.; Dussarat, A.; Fromentin, C.; Goin D'Ambrières, S.; Lachaud, S.; Laurin, P.; Le Martret, O.; Loyau, V.; Tessot, N.; Pejac, J. M.; Perron, S. *Bioorg. Med. Chem. Lett.* **1999**, *9*, 3075.
2. Cachet, T.; Van den Mooter, G.; Hauchecorne, R.; Vinckier, C.; Hoogmartens, J. *Int. J. Pharm.* **1989**, *55*, 59.
3. Agouridas, C.; Collette, P.; Mauvais, P.; Chantot, J. F. *34th Interscience Conference on Antimicrobial Agents and Chemotherapy*, 1994; F-166.
4. Agouridas, C.; Benedetti, Y.; Denis, A.; Le Martret, O.; Chantot, J. F. *35th Interscience Conference on Antimicrobial Agents and Chemotherapy*, 1995; F-157.
5. Agouridas, C.; Denis, A.; Auger, J. M.; Benedetti, Y.; Bonnefoy, A.; Bretin, F.; Chantot, J. F.; Dussarat, A.; Fromentin, C.; Goin D'Ambrières, S.; Lachaud, S.; Laurin, P.; Le Martret, O.; Loyau, V.; Tessot, N. *J. Med. Chem.* **1998**, *41*, 4080.
6. Ednie, L. M.; Spangler, S. K.; Jacobs, M. R.; Appelbaum, P. C. *Antimicrob. Agents Chemother.* **1997**, *41*, 1033.
7. Ednie, L. M.; Spangler, S. K.; Jacobs, M. R.; Appelbaum, P. C. *Antimicrob. Agents Chemother.* **1997**, *41*, 1037.
8. Jamjiam, C.; Biedenbach, D. J.; Jones, R. N. *Antimicrob. Agents Chemother.* **1997**, *41*, 454.
9. Bertho, G.; Gharbi-Benarous, J.; Delaforge, M.; Lang, C.; Parent, A.; Girault, J. P. *J. Med. Chem.* **1998**, *41*, 3373.
10. Agouridas, C.; Bonnefoy, A.; Chantot, J. F. *35th Interscience Conference on Antimicrobial Agents and Chemotherapy*, 1995; F-158.

11. Delaforge, M.; Sartori, E. *Biochem. Pharmacol.* **1990**, *40*, 223.
12. Goldman, R. C.; Fesik, S. W.; Doran, C. C. *Antimicrob. Agents Chemother.* **1990**, *34*, 426.
13. Fernandez-Munoz, R.; Vazquez, D. *J. Antibiot.* **1973**, *26*, 107.
14. Pestka, S. *Antimicrob. Agents Chemother.* **1974**, *6*, 474.
15. Agouridas, C.; Benedetti, Y.; Denis, A.; Fromentin, C.; Gouin d'Ambrières, S.; Le Martret, O.; Chantot, J. F. *34th Interscience Conference on Antimicrobial Agents and Chemotherapy*, 1994; F-164.
16. Gyi, J. I.; Brennan, R. J.; Pye, D. A.; Barber, J. *J. Chem. Soc., Chem. Commun.* **1991**, 1471.
17. Brennan, R. J.; Awan, A.; Barber, J.; Hunt, E.; Kennedy, K. L.; Sadegholnejat, S. *J. Chem. Soc., Chem. Commun.* **1994**, 1615.
18. Barber, J.; Gyi, J. I.; Pye, D. A. *J. Chem. Soc., Chem. Commun.* **1991**, 1249.
19. Balaram, P.; Bothner-By, A. A.; Dadok, J. *J. Am. Chem. Soc.* **1972**, *94*, 4015.
20. Balaram, P.; Bothner-By, A. A.; Breslow, E. *J. Am. Chem. Soc.* **1972**, *94*, 4017.
21. Bothner-By, A. A.; Gassend, R. *Ann. N. Y. Acad. Sci.* **1973**, *222*, 668.
22. Gronenborn, A. M.; Clore, G. M.; Blazy, B.; Baudras, B. *FEBS Lett.* **1981**, *136*, 160.
23. Clore, G. M.; Gronenborn, A. M. *J. Magn. Reson.* **1982**, *48*, 402.
24. Campbell, A. P.; Sykes, B. D. *J. Magn. Reson.* **1991**, *93*, 77.
25. Bertho, G.; Gharbi-Benarous, J.; Ladam, P.; Delaforge, M.; Girault, J. P. *Bioorg. Med. Chem.* **1998**, *6*, 209.
26. Awan, A.; Brennan, R. J.; Regan, A. C.; Barber, J. *J. Chem. Soc., Chem. Commun.* **1995**, *16*, 1653.
27. Homann, H. E.; Nierhaus, K. H. *Eur. J. Biochem.* **1971**, *20*, 249.
28. Verdier, L.; Bertho, G.; Gharbi-Benarous, J.; Girault, J.-P. *Bioorg. Med. Chem.* **2000**, *8*, 1225.
29. Vannuffel, P.; Di Giambattista, M.; Morgan, E. A.; Cocito, C. *J. Biol. Chem.* **1992**, *267*, 8377.
30. Vannuffel, P.; Cocito, C. *Drugs* **1996**, *51* (Suppl. 1), 20.
31. Di Giambattista, M.; Engelborghs, Y.; Nyssen, E.; Cocito, C. *J. Biol. Chem.* **1987**, *262*, 8591.
32. Chang, F. N. *Lincomycin*; Hahn, F. E., Ed.; New York, 1979; Vol. 5.
33. Contreras, A.; Vazquez, D. *Eur. J. Biochem.* **1977**, *74*, 539.
34. Bax, A.; Davis, D. G. *J. Magn. Reson.* **1985**, *65*, 355.
35. Bendall, M. R.; Pegg, D. T. *J. Magn. Reson.* **1983**, *53*, 272.
36. Bax, A.; Summers, M. F. *J. Am. Chem. Soc.* **1986**, *108*, 2093.
37. Rutar, A. *J. Magn. Reson.* **1984**, *59*, 306.
38. Ladam, P.; Gharbi-Benarous, J.; Piotto, M.; Delaforge, M.; Girault, J. P. *Magn. Reson. Chem.* **1994**, *32*, 1.
39. Haasnoot, C. A. G.; De Leeuw, F.; Altona, C. *Tetrahedron* **1980**, *36*, 2783.
40. Tvaroska, I.; Hricovini, M.; Petrakova, E. *Carbohydrate Research* **1989**, *189*, 359.
41. Allerhand, A.; Doddrell, D.; Komoroski, R. *J. Chem. Phys.* **1971**, *55*, 189.
42. Dinur, U.; Hagler, A. T. *J. Chem. Phys.* **1992**, *97*, 9161.
43. Dauber-Osguthorpe, P.; Roberts, V. A.; Osguthorpe, D. J.; Wolff, J.; Genest, M.; Hagler, A. T. *Proteins: Structure, Function and Genetics* **1988**, *4*, 31.
44. London, R. E.; Perlman, M. E.; Davis, D. G. *J. Magn. Reson.* **1992**, *97*, 79.
45. Clore, G. M.; Gronenborn, A. M. *J. Magn. Reson.* **1983**, *53*, 423.
46. Wuthrich, K.; Billeter, M.; Braun, W. *J. Mol. Biol.* **1983**, *169*, 949.
47. Retsema, J. A.; Girard, A. E.; Schekly, W.; Manousos, M.; Anderson, M. R.; Bright, G. M.; Borovoy, R. J.; Brennan, L. A.; Mason, R. *Antimicrob. Agents Chemother.* **1987**, *31*, 1939.
48. Bertho, G.; Ladam, P.; Gharbi-Benarous, J.; Delaforge, M.; Girault, J. P. *Int. J. Biol. Macromolecules* **1998**, *22*, 103.
49. Bertho, G.; Ladam, P.; Gharbi-Benarous, J.; Delaforge, M.; Girault, J. P. *J. Chim. Phys.* **1998**, *95*, 423.
50. Agouridas, C.; Collette, P.; Mauvais, P.; Chantot, J. F. *35th Interscience Conference on Antimicrobial Agents and Chemotherapy,* 1995; F-170.
51. Dinur, U.; Hagler, A. T. *J. Chem. Phys.* **1989**, *91*, 2949.
52. Berendsen, H. J. C.; Postma, J. P. M.; Gunsteren, W. F. v.; DiNola, A.; Haak, J. R. *J. Chem. Phys.* **1984**, *81*, 3684.
53. Jelenc, P. *Anal. Biochem.* **1980**, *105*, 369.